NUMERICAL ESTIMATION AND EXPERIMENTAL COMPARISON OF VORTEX-INDUCED VIBRATION FATIGUE IN MARINE RISERS

A Thesis

by

CHETNA PRAKASH KAMBLE

Submitted to the Office of Graduate and Professional Studies of
Texas A&M University
in partial fulfillment of the requirements for the degree of

MASTER OF SCIENCE

Chair of Committee,	Hamn-Ching Chen
Committee Members,	Kuang-An Chang
	Alan Palazzolo
Head of Department,	Sharath Girimaji

May 2016

Major Subject: Ocean Engineering

ABSTRACT

Advancement in computational sciences has made Computational Fluid Dynamics an attractive alternative to simulate fully three dimensional VIV motion for very long marine risers (L/D > 1000). In this study, an unsteady Finite Analytic Navier-Stokes (FANS 3D) method has been applied in conjunction with Large Eddy Simulation (LES) to simulate the flow field around the risers. The riser has been modeled as a tensioned beam and a beam motion equation is employed to calculate the riser displacements. This equation has been discretized using finite difference scheme and is coupled with the FANS 3D solver using a feedback loop to achieve Fluid Structure Interaction (FSI). The riser and flow field are decomposed in two structured grids and the chimera (overset) grid technique is utilized to achieve interpolation between the overlapping grid regions. A modal strain calculation method is developed to extract the strain time series from riser displacements and the rainflow counting algorithm is employed to estimate fatigue damage associated with different riser and current profiles.

VIV fatigue analysis of two riser geometries with L/D ≈ 1400 from NDP 2003 experiments and L/D ≈ 4200 from DeepStar Miami2 2006 experiments, has been conducted. The riser from NDP experiments is placed horizontally and is subjected to uniform and linearly sheared current profiles. A highly-sheared (non – uniform) current is specified to the riser from Miami2 experiments. The results obtained from CFD simulations are compared to the experimental results and published data to verify the accuracy of the flow field solver, riser motion solver and fatigue calculation module.

DEDICATION

This thesis is dedicated to my mother, Rajani, for her unwavering support all these years of my life, my father, Prakash, who always believed in me and is still watching over me from the heaven above and to my partner in crime, Ashwin, for all his love and guidance throughout my graduate life.

.

ACKNOWLEDGEMENTS

I would like to offer my sincere gratitude to my committee chair, Dr. H.C. Chen for his continuous support and encouragement throughout the course of this research. It was a privilege working under his guidance and his constant motivation inspired me to pursue my thesis with great dedication. I would also like to thank my committee members, Dr. Kuang-An Chang and Dr. Alan Palazzolo for their valuable inputs and suggestions during the course of this thesis.

I would also like to take this opportunity to thank the Department of Ocean Engineering at Texas A&M University for facilitating my research work and making my graduate life a wonderful experience. A very special acknowledgement goes to Laura Byrd for helping me with all the necessary formalities and paperwork during the course of my graduate study.

I want to extend my gratitude to Norwegian Deepwater Programme (NDP) and DeepStar for releasing the experimental datasets which were essential for this research. Finally, I want to thank everyone involved in making my research a success.

NOMENCLATURE

CFD	Computational Fluid Dynamics
VIV	Vortex-induced Vibration
L	Length of the riser
D	Outer diameter of the riser
FANS	Finite Analytic Navier Stokes
LES	Large Eddy Simulation
T	Tension in the riser
FSI	Fluid Structure Interaction
V	Velocity
t	Time Step
3D	Three Dimensional
2D	Two Dimensional
Z	Crossflow Direction
Y	Inline Direction
RFC	Rainflow Counting Algorithm
PSD	Power Spectral Density
nx	n^{th} harmonic of fundamental frequency
RMS	Root Mean Square

TABLE OF CONTENTS

Page

LIST OF FIGURES

Page

LIST OF TABLES

Page

CHAPTER I

INTRODUCTION AND LITERATURE REVIEW

Vortex-induced vibrations (VIV) are becoming an increasingly popular field of research in offshore engineering. With the deepest platforms now located at nearly 30000ft in the Gulf of Mexico, the slender structures typically marine risers, pipelines, tendons and mooring lines are adversely affected by the harsh marine environment. These flexible bodies experience VIV induced fatigue damage when exposed to strong sea currents, which occurs due to periodic shedding of vortices with opposite signs from the aft of the marine riser. The vortex induced vibrations are an immediate threat to the structural integrity of the system. The wear and tear caused by the VIV induced fatigue can lead to collapse of the riser thereby exposing potential environmental risks. Therefore, accurate prediction of the fatigue life is of prime importance to prevent accidents and monetary losses.

Much of the understanding about Vortex-Induced Vibrations is derived from Blevins (1990), Bearman (1984), Pantazopoulos (1994), Newman (1997) and Saprkaya (1989). Last decade saw numerous publications which presented valuable insights of the VIV phenomenon including Govardhan and Williamson (2004) which discussed frequency response of elastically mounted cylinder and Bourget et al. (2011) which primarily dealt with the lock-in phenomenon associated with VIV. All these publications have led to significant breakthroughs in successful modelling of the VIV in flexible marine structures. Model testing and full scale experiments have been carried out to

perfectly predict the complex nature of vortex-induced vibrations associated with slender bodies. Experiments conducted at Hanoytangen in 1997 (Lie and Kassen, 2006) used a 90m long tensioned riser in shear flow to study both crossflow and inline motions occurring at high mode numbers. British Petroleum (Tognarelli et al. 2008) used in-situ measurements to calculate the fatigue damage based on field acceleration data which presented a realistic view of VIV occurring in drilling risers. Commercial software such as Shear7 (Vandiver and Lee, 2003) and VIVA (Triantafyllou et al., 2003) have used such experimental data to generate empirical models which calculate the transverse response of VIV motion quite accurately.

Due to increasing costs of sensor installations on deep marine risers and severe constraints on experimental facilities owing to increasingly large water depth, numerical methods for VIV prediction have gained popularity in recent years. Computational fluid dynamics has become very feasible in recent years due to advancement in computational sciences. Millions of grid points are now being easily handled by supercomputers which is extremely essential for modelling the three dimensional nature of VIV accurately. Recent publications in numerical simulation of riser VIV include Newman and Karniadakis (1997) who used laminar flow velocity regions (Re = 100 to 300) on a flexible body with a low L/D ratio to quantify coupled fluid-structure response. Meneghini et al. (2004) employed a discrete vortex method (DVM) to estimate the fluid forces on slender bodies. Lucor et al. (2006) applied a low resolution Direct Numerical Simulation (DNS) to predict modal amplitude response of very long riser (L/D = 2000) in sheared flow (Re = 1000) which resulted in prediction of travelling waves at high

velocity regions. Holmes et al. (2006) presented a fully three dimensional CFD simulation of a riser of length 38 m using Galerkin/Least-Squares based finite element CFD solver. Pontaza, Chen and Chen (2005) used the overset (chimera) grid system to solve Navier-Stokes equations at Re = 10^5 and presented the VIV response of risers in tandem. Thus, VIV phenomenon has been extensively studied using both experimental and numerical approach and many critical aspects of it have been explained. However, the complexity of these vibrations on marine structures leaves a lot of room for further research in this field.

Due to deeper oil explorations and significant advancements in offshore industry flexible marine bodies are subject to extended periods of operation in severe environment which causes rapid accumulation of fatigue damage. This has led to VIV fatigue being a very important aspect in marine risers. Norwegian Deepwater Program (NDP) conducted a series of experiments on a riser with L/D ~ 1400 to study both inline and crossflow fatigue. The results were published in Trim et al. (2005) and shed significant light on fatigue damage occurring at different locations on the riser. Mukundan et al. (2009) used these results to reconstruct the VIV fatigue response and compared it with fatigue estimates from Van der wake oscillator model. Thorsen et al. (2015) have also used the same experiments to generate fatigue damage by using a semi empirical time domain simulation of VIV. A hydrodynamic force model and Euler-Bernoulli beam equation model have been used to represent the fluid and structure respectively. These studies have established the importance of inline fatigue which is comparable to its crossflow counterpart (Baarholm et al., 2006) and which is generally

neglected in commercial VIV analysis packages. Another realistic experiment (Miami 2006) for very long riser (L/D ~ 4200) was conducted in Gulf of Mexico by DeepStar. This experiment involved VIV analysis of a riser in a non-uniform flow. The results were analyzed by Vandiver et al. (2006) and Jhingran et al. (2007) to estimate fatigue damage occurring in the riser due to excitation of higher harmonics. Constantinides and Oakley (2008) have used the Miami experiments to predict the fatigue damage from 1st harmonic and 3rd harmonic of the strain signals using CFD. It was concluded that higher harmonics could be captured in future by rapidly increasing computational capabilities.

This thesis presents an estimation of fatigue damage associated with crossflow and inline VIV via an overset (Chimera) grid domain decomposition method using Finite Analytic Navier Stokes (FANS) flow field solver for very long marine risers. This method has been adopted by Huang, Chen and Chen (2007, 2008, 2010, 2011, and 2012) to predict the vortex-induced vibration in slender structures. The results published show a significant correlation between the CFD simulations and the experimental analysis. During the course of this thesis, a similar comparison is made for riser geometries extracted from NDP 2003 and Miami 2006 experiments. The FANS CFD algorithm is applied to risers with L/D ~ 1400 and L/D ~ 4200 in uniform, sheared and non-uniform current profiles and the results are compared with field data. A fatigue analysis module is developed to use rainflow counting algorithm to predict the fatigue damage associated with the riser in-line and crossflow motion. The fatigue life results are compared with experimental results are valid conclusions are drawn

CHAPTER II

NUMERICAL APPROACH

FANS Flow Field Solver

A Finite Analytic Navier-Stokes (FANS 3D) algorithm is applied to simulate the flow field around the riser. The method has been developed in Pontaza, Chen and Chen (2004, 2005a, 2005b), Pontaza, Chen and Reddy (2005) and Pontaza and Chen (2007). This main composition of the algorithm is described as follows:

- The exact analytical solution for the locally linearized governing differential equations in the form of Fourier series is acquired.
- The whole numerical domain is divided in smaller sections and the analytical solution is applied to each node locally in algebraic form providing inter-nodal connections.
- The local analytical equations are then used to form a system of equations and each nodal value is resolved and the solution for the whole domain is thus obtained.

In the FANS 3D solver the governing equations are constituted of unsteady three-dimensional Navier Stokes Equations. The continuity equation for the fluid flow is solved using a finite volume scheme. The turbulence associated with the vortices formed at the aft of the riser is solved using large eddy simulation (LES) method. This method is based on volume-averaging of the Navier Stokes equation to filter out the small scale

vortices from the solutions which are considered to have negligible contribution towards vortex induced vibrations. This is done to reduce the computational cost and improve efficiency of the overall problem. LES uses following differential equation (Eq. (1)) for modelling turbulent flow:

$$\frac{\partial \overline{u}_i}{\partial t} + \frac{\partial}{\partial x_j}(\overline{u}_i \overline{u}_j) = -\frac{1}{\rho}\frac{\partial \overline{p}}{\partial x_i} + \nu \frac{\partial^2 \overline{u}_i}{\partial x_i \partial x_j} - \frac{\partial \tau_{ij}}{\partial x_i} \tag{1}$$

The subgrid stresses τ_{ij} are resolved using Smagorinsky's subgrid-scale turbulence model as given in Eq. (2) below where $\overline{S}_{ij}$ represents the local strain tensor. The Smagorinsly's coefficient is represented by C_s. Damping is neglected in this method and all the vortices with sizes below the grid size Δ are filtered out for rapid calculations.

$$\left.\begin{aligned} \tau_{ij} &= \overline{u_i u_j} - \overline{u}_i \overline{u}_j \\ \tau_{ij} &= -2\nu_t \overline{S_{ij}} \\ \nu_t &= (C_S \Delta)^2 \sqrt{2\overline{S}_{ij}\overline{S}_{ij}} \\ S_{ij} &= \frac{1}{2}\left(\frac{\partial \overline{u_i}}{\partial x_j} + \frac{\partial \overline{u_i}}{\partial x_i}\right), \\ \Delta &= (\Delta_x \Delta_y \Delta_z)^{1/3} \\ Cs &= 0.1 \end{aligned}\right\} \tag{2}$$

The pressure-velocity coupling is resolved using a hybrid PISO/SIMPLER and the pressure field is continuously updated. This method also requires the governing equations to be transformed from Cartesian space to numerical space with ξ, η, γ coordinates. Application of this method for Reynold's numbers upto 10^7 has been verified through results published by Pontaza, Chen & Reddy (2005) and which makes it

applicable to the analyses in this study. The coordinate system for riser VIV analysis is shown in Fig. 1 where x axis is along the riser axial direction, y axis is along the incoming velocity direction and z axis is in the crossflow direction.

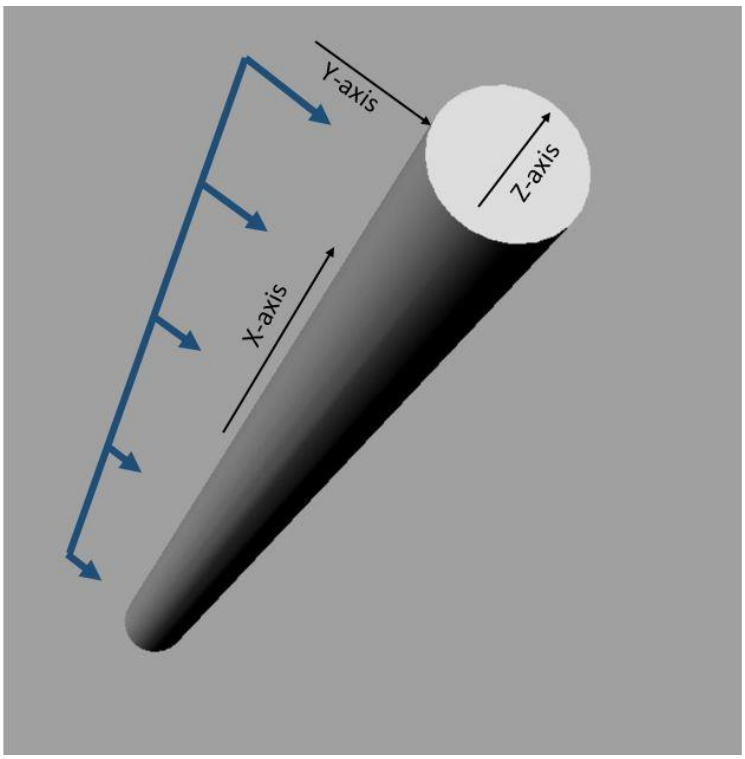

Figure 1. Riser coordinate system

Riser Motion Solver

Deepwater risers are slender flexible conduits which are used for transport of fluids through the water column to offshore platforms, in the oil and gas industry. These

risers are generally tensioned at top with little flexural rigidity. In our problem, the risers have been modeled as an axially tensioned beam and the beam motion equation has been derived from the Euler Bernoulli beam theory. Vortex-induced vibrations generally invoke small transverse motions in the risers compared to wavelength and are generally comparable to the characteristic outer diameter of the riser (a/D ≈ 1) and therefore the structural model is linearized with variable tension and stiffness.

Eq. (3) representing the in-line response of the riser are given below:

$$T\frac{d^2y}{dx^2}+\frac{dy}{dx}\frac{dT}{dx}-\frac{d^2}{dx^2}\left(EI\frac{d^2y}{dx^2}\right)+f_y=m\ddot{y}+D_s\dot{y} \tag{3}$$

The first three terms in (3) and (4) above are stiffness terms where T represents effective tension in the beam and EI represents the flexural rigidity of the beam, f_y represents the external forces acting on the beam. In this study the external forces will comprise of the hydrodynamics forces generated via the FANS CFD algorithm. The mass of the beam is represented by m and D_s is the damping coefficient in the motion equation. The damping is generally neglected in the deepwater marine riser analysis for simplification purposes. Since the risers are very slender structures, the flexural rigidity can be neglected as it has extremely small influence on risers vibrating at lower modes with high axial tensions. As a results in the solution analysis $EI \approx 0$ and therefore the Eq. (3) can be simplified in to Eq. (4) which has analytical modal solutions.

$$T\frac{d^2y}{dx^2}+\frac{dy}{dx}\frac{dT}{dx}+f_y=m\ddot{y} \tag{4}$$

Another method to solve the above equations has been developed by Huang, Chen and Chen (2011) and it is shown to be unconditionally stable. This method uses an implicit finite difference scheme which uses a direct integration approach at each time step. The riser is assumed to start from a stationary position and therefore the initial conditions are set to be zero. Also, the riser is pinned at both the ends and a zero motion boundary conditions is applied on both ends. The final finite differentiated equation of the riser motion is presented in Eq. (5).

$$\frac{EI}{l^4}y_{j-2}^n-\left(\frac{T_j}{l^2}-\frac{w_j}{2l}+\frac{4EI}{l^4}\right)y_{j-1}^n+\left(\frac{2T_j}{l^2}+\frac{D_s}{\tau}+\frac{6EI}{l^4}+\frac{m}{\tau^2}\right)y_j^n$$
$$-\left(\frac{T_j}{l^2}+\frac{w_j}{2l}+\frac{4EI}{l^4}\right)y_{j+1}^n+\frac{EI}{l^4}y_{j+2}^n=f_{yj}^n+\left(\frac{D_s}{\tau}+\frac{2m}{\tau^2}\right)y_j^{n-1}-\frac{m}{\tau^2}y_j^{n-2} \quad (5)$$

In the equation above l represents the riser section length and τ represents the time step for the iteration. Note that all the equations are written and simplified in crossflow (z) direction in a similar fashion. Please refer to Huang, Chen and Chen (2011) for more details regarding the discretization process.

Fluid structure interaction is achieved by coupling the riser motion solver and FANS CFD flow field solver using a feedback loop. Initially the lift coefficient C_l and drag coefficient C_d are calculated using FANS algorithm. These coefficients are then applied to obtain external hydrodynamic force acting on the riser. These forces are used to obtain riser crossflow (z) and in-line (y) displacements for each time step. These displacements are then treated as boundary conditions for the riser and again looped back to the flow field solve to generate new force coefficients.

Fatigue Calculation Module

The main contribution to the riser fatigue is from the Vortex Induced Vibrations engendered from generation of oscillating forces on riser due to vortex shedding. These oscillations take place at high frequencies and can be of an order equivalent to the riser diameter. The fatigue damage due to these vibrations accumulates over a period of time and can lead to the eventual failure of the structure. Fatigue calculation from the generated strain time series is done using a Rainflow Counting Algorithm. This method was developed by T.Endo and M. Matsuishi in 1968 by studying the raindrops flowing down from a "Pagoda" roof. This time domain method calculates fatigue from stress time histories using simple stress reversals.

Rainflow counting algorithm uses few simple rules to estimate cycles associated with each stress range ΔS.

- Each rainflow drop begins at the start of the time series and from each +ive stress amplitude (peak) and negative amp (valley)
- The raindrop falls down until it reaches a more +ive peak (or more –ive valley) than from initial starting peak (or valley)
- The raindrop terminates when it merges with any raindrop falling from the above peak or valley.
- The raindrop also terminates at the end of time history

Fig. 2 depicts the flowchart adopted in development for the rainflow counting algorithm (RFC) for FANS CFD solver. The damage caused by each cycle is calculated by referring to the S-N Curve. The S-N Curve shows the number of Cycles to failure N_f for a given stress range S. The total damage by N number of cycles is obtained as the ratio of the cycles from the actual stress time history to the number cycles to failure. The above rule is called Miner's rule and is widely used in the industry.

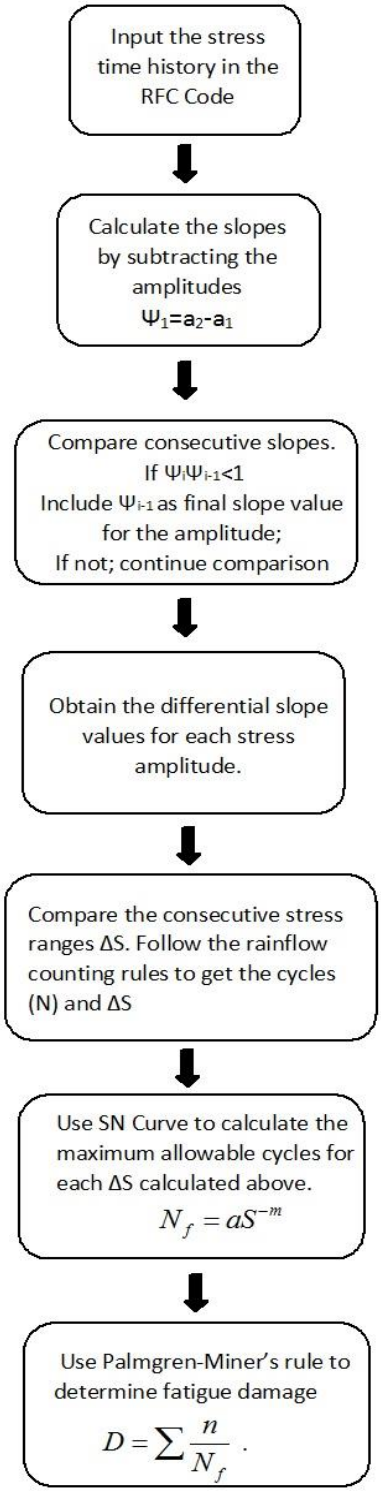

Figure 2. Flowchart of the rainflow counting algorithm (RFC)

The Rainflow Counting Algorithm has been verified by application to a random stress cycle and comparing the results with *StoFlo*^{TM} a rainflow counting excel database with enabled Macros. Fig. 3 depict the stress cycle for which the cycle counting assessment has been done. Fig. 4 states the probability density function from both the RFC generated for the FANS CFD solver and *StoFlo*^{TM}.

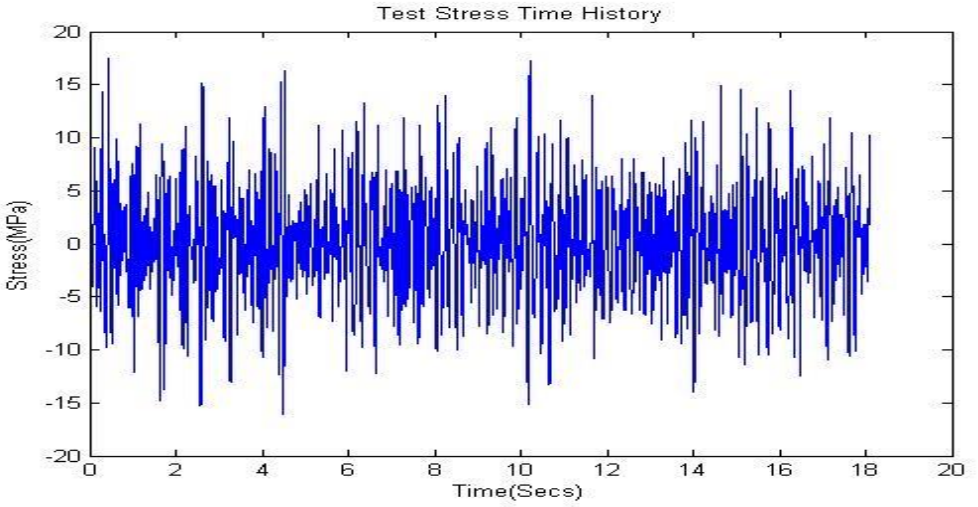

Figure 3. Test stress time history used for verification of RFC numerical code

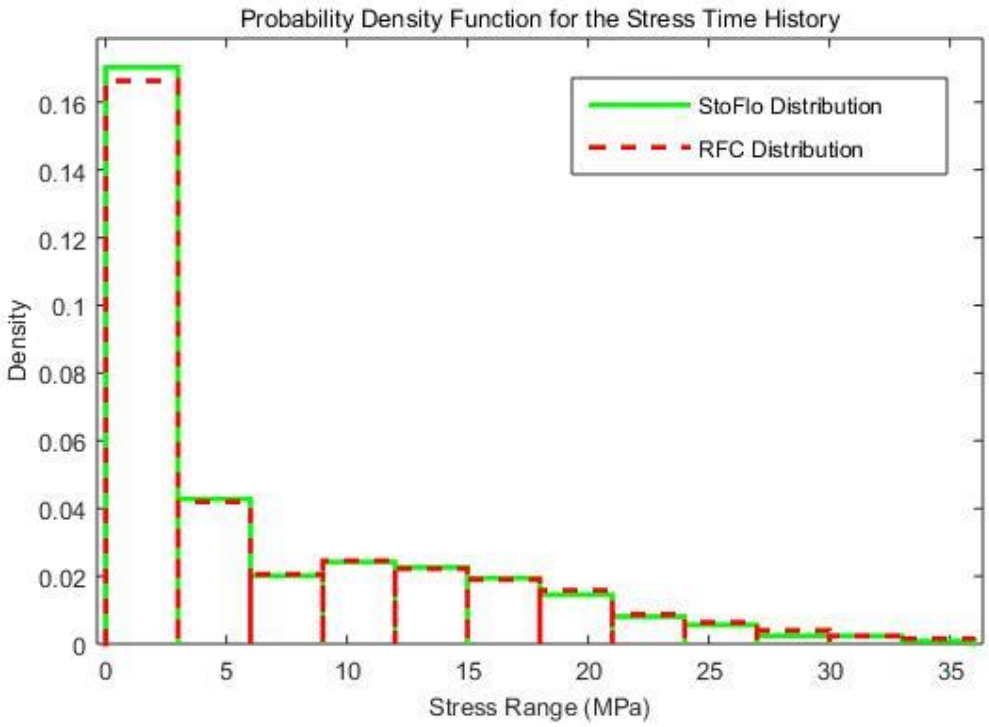

Figure 4. Probability density functions generated by RFC and *StoFlo*^{TM}

Data Grid Description

Computational Fluid Dynamics has become extremely vital in handling complex flow structure interaction problems and has made significant advances in recent years due to increase in computational speeds and efficiency. The meshing techniques have become very convenient as the computers are able to handle millions of grid points easily. Unstructured grids have been very popular in CFD simulations and have been widely applied in solving various complex flow problems. However, their drawbacks include subpar accuracy with many solvers, inclusion of more number of grid points in

boundary layers than the structured grids and difficulty in modeling moving or deforming boundaries. Structured grids are much more accurate with CFD solvers and are more highly efficient with space. Nevertheless they are extremely difficult to use while meshing highly complicated structures.

Overset (Chimera) grids are much more flexible with modelling intricate details of various engineering structures. This grid system consists of block structured grids with overlapping blocks. The flow information is exchanged between the grids by interpolating solutions in the overlapped region. Grid points not used in the solution (hole points) are removed from the system which lowers the cell count and generates a high quality mesh. The overset grid system consists of a near body curvilinear grid and an off-body Cartesian grid. Both surface grids and volume grids have to be generated for the system. Next step involves identifying the grid points that fall inside the solid boundaries which is termed as 'hole cutting'. Once the points have been removed adjustments are made to the boundaries of the resulting holes to facilitate inter-grid data exchange. The last step in domain connectivity is to search for interpolation stencils for fringe points which are located in the interior of the neighboring blocks and require information from that containing block. Overset grid offers efficiency by allowing the change in one grid without affecting the other grid systems. This is extremely important in a multiple grid system where the effect of grid resolution has to be studied on a particular grid.

Fig. 5 represents the overset grid system which will be used in this study. The grid in red is a body fitted curvilinear grid for the riser structure whereas the grid in

green is the body-off (background) grid in Cartesian coordinates. In a problem with multiple structures, a curvilinear grid can be generated for each structure and embedded in the body-off (background) grid. The flow information is exchanged between both the grids by interpolation of flow variables.

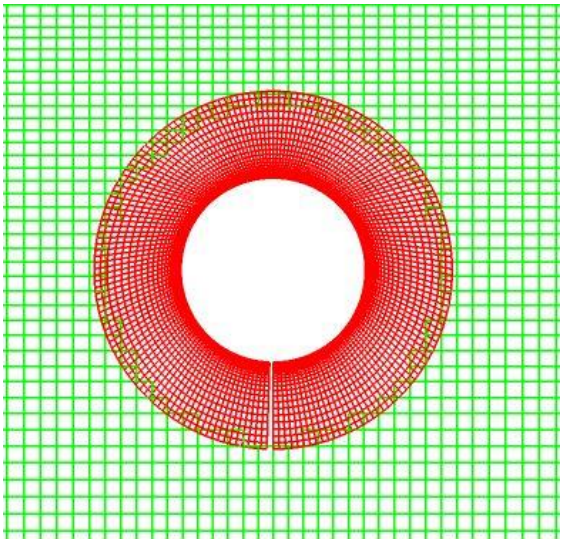

Figure 5. Overset grid cross-sectional view

In this study, a program called PEGSUS (Suhs et al., 1991) was employed to identify the hole points and determine the interpolation weights. Fig. 6 shows the hole cutting as performed by PEGSUS and hole points and fringe points are marked.

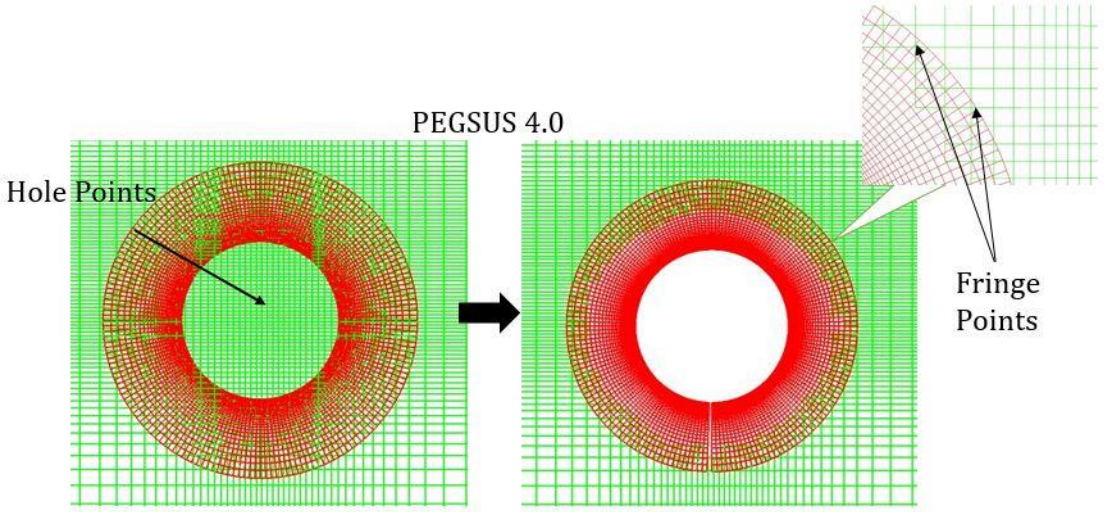

Figure 6. Overset grid generation by PEGSUS

The grid system used in this thesis consists of two major grids, riser grid and wake grid.

a) Riser Grid: The body grid is the grid adjacent to riser which is used to calculate the fluid riser interaction and vortex formation.
b) Wake Grid: Wake grid is the interface between the riser and the background flow field which is used to get the enhanced resolution for the vortex shedding from the aft of the riser

The system described above is represented in Fig. 7 where the red circular curvilinear grid is the body fitted riser grid and the wake grid is the green rectangular grid embedding the riser grid. It can be deduced from the figure that the resolution around the riser and to a certain distance aft from the riser is extremely fine. This is an essential requirement of precise determination of vortex formation from the aft of the riser. The grid cells far away from the riser have coarse resolution as the solutions at those

locations do not affect the VIV solutions and don't hurt the accuracy of overall simulation. The embedding region between the riser and wake grids is used to interpolate the flow information as mentioned above.

The riser and wake grid shown above are cross-sectional grids specified at each axial location on the riser. A full 3D view of the grids used in the VIV analysis is presented in Fig. 8. The riser is divided into finite segments in axial direction which are generally small for low velocities as the solution is not affected by quality of axial resolution (Huang Chen and Chen 2007). However at higher velocities and for long risers the flow field changes significantly over the length of riser in axial direction and therefore a much finer axial resolution is required to accurately describe the flow field.

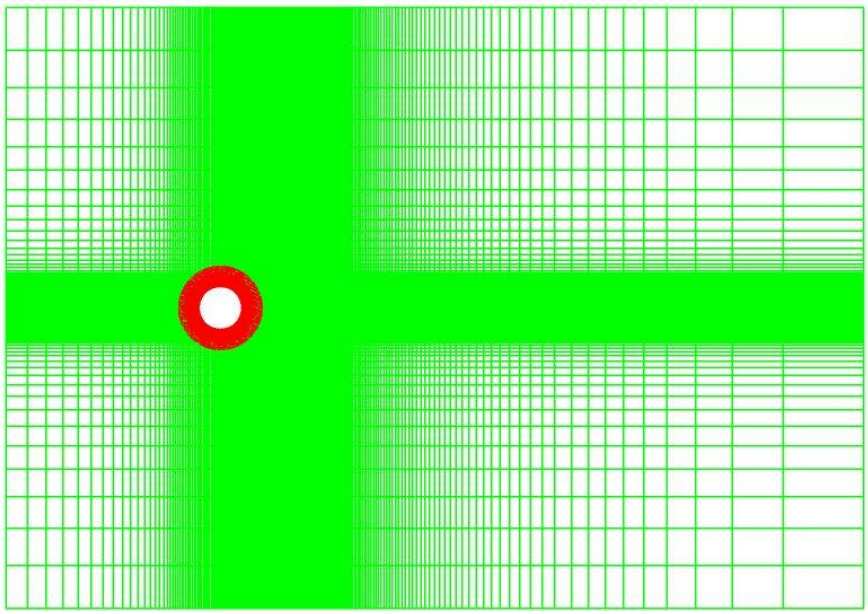

Figure 7. Cross-section of the grids used in VIV analysis

FANS 3D and Riser Motion Solver algorithm allow flexibility in the choice of axial segmentation of the riser and the flow field in the vicinity of the riser. The lift (C_l) and drag (C_d) coefficients calculated at the fluid axial segments by the FANS 3D solver are mapped to the structural segments leading to Fluid-Structure Interaction (FSI). Normally, finer axial structural mesh is applied to capture the curvature and motion data accurately. Segmentation of the flow field near the riser is kept coarse as the flow field varies smoothly along the length of the riser.

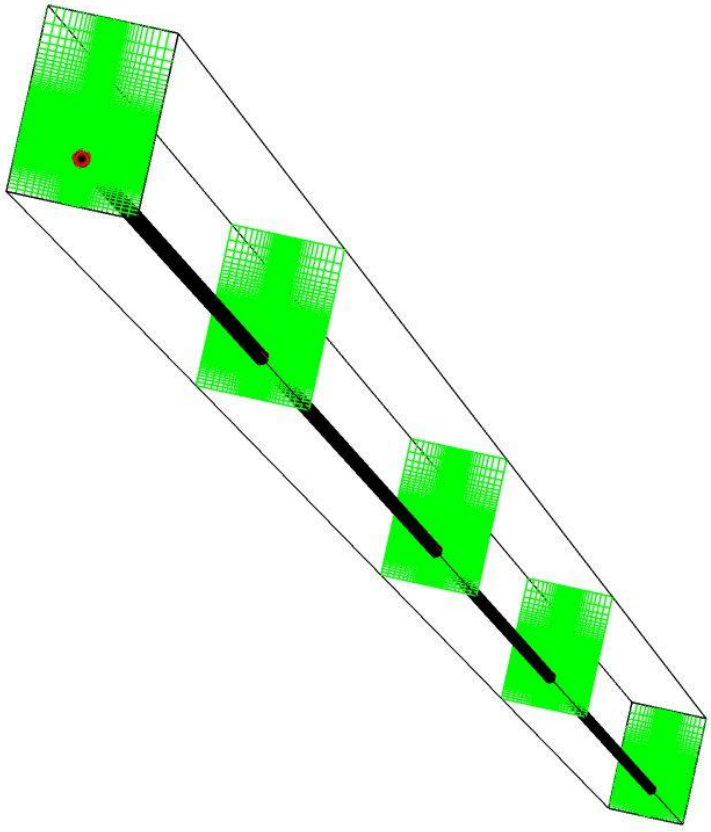

Figure 8. 3D grid system used in VIV analysis

CHAPTER III

RISER IN UNIFORM CURRENTS

In this section, VIV fatigue analysis of a horizontal riser with length of 38 m and outer diameter of 0.027 m in uniform current velocities of 0.3 m/s, 0.7 m/s, 1.4 m/s and 1.7 m/s is discussed. The riser geometry is derived from NDP 2003 experiments and a comparison of fatigue data has been made between the simulations and experiments.

Experimental Setup

Norwegian Deepwater Programme (NDP) conducted a series of high mode VIV tests in MARITEK'S offshore basin in Trondheim in December 2003. Both bare riser and straked riser geometries were studied. In this thesis only bare riser tests are used for VIV analysis. These tests were performed with the objective of obtaining data to improve understanding of high mode VIV for long riser like cylinders. The riser was towed at a constant speed to generate a uniform flow profile. The end terminations of the riser were secured firmly to limit the vibrations which could corrupt the results. A clump weight spring system was attached at each end of the riser model suspended by an inclined pendulum. The upper end of the pendulum was tugged using a gondola (transverse crane system). The pendulum was used to curb the rotations from the clump weight to the riser. The riser was fitted with 40 inline strain gauges and 23 to 24 crossflow strain gauges to record the strain time histories which were used for fatigue

processing. A set of 8 accelerometers in the inline and crossflow directions were also used for comparison of strain regenerated motion time histories. A weight of 4-6 kN was attached at both ends of the riser to provide required tension. Deepwater risers in high current velocities are tension dominated. To reduce flexural stiffness effect while calculating the bending modes of the riser, a fiberglass material was used to build the pipe. The mass ratio (total mass flooded divided by displaced mass) of the riser was calculated to be 1.62 and was used in subsequent calculations. The experimental setup is presented in Fig. 9 and the physical properties of the riser can be found in Table 1.

Physical Property	Value
Length overall	38.0 m
Outer Diameter	27 mm
Wall thickness	3.0 mm
Bending Stiffness, EI	37.2 Nm^2
Young Modulus for pipe, E	2.2 X 10^9 N/m^2
Axial stiffness, EA	5.09 X 10^5 N
Mass of the pipe (air filled)	0.761 kg/m
Mass of the pipe (water filled)	0.933 kg/m
Mass ratio	1.62
Effective tension	5000 N

Table 1. Physical properties of bare riser from NDP 2003 experiments

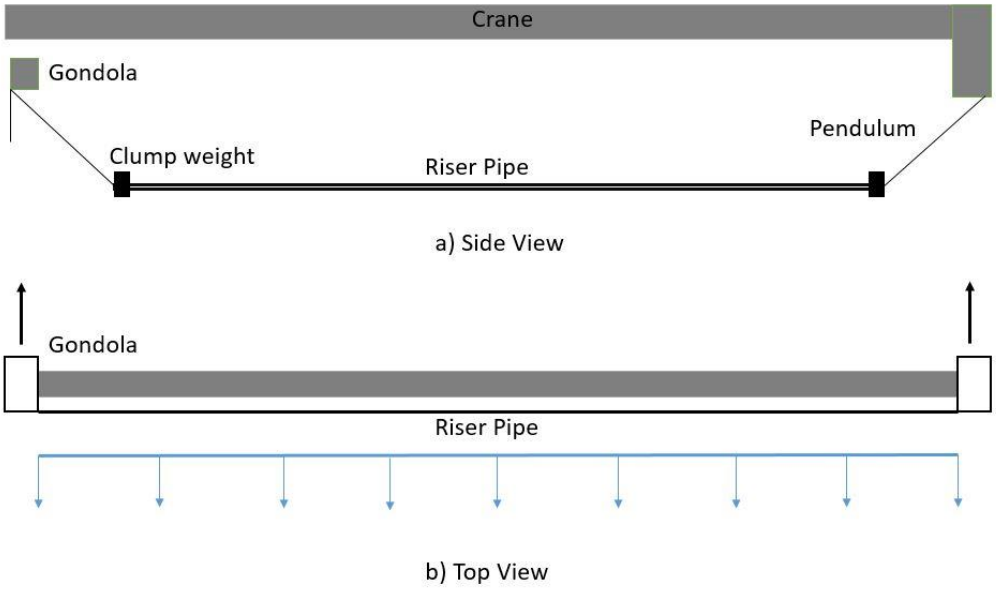

Figure 9. Experimental setup for uniform current from NDP expts (Trim et al., 2005)

Numerical Simulation Results

The riser geometry studied in this section has L/D = 1400 which is typical for a riser employed in deep-water offshore rigs. The simulation uses a FANS CFD solver and coupled riser motion solver to generate the inline and crossflow motion time histories. These time histories are later processed to generate stress time series which are converted to VIV fatigue damage via rainflow counting. The numerical grid consists of 1.3 million grid points and has a body gird resolution of 100 axial sections, 182 circumferential sections and 41 radial sections. The body grid is used to model the VIV analysis for the riser by predicting the instantaneous riser motion. The wake grid or

background grid has dimensions of 100 axial sections, 101 circumferential sections and 51 radial sections. The overlapping region between the two grids is used to interpolate the flow information between them.

The riser is subjected to a uniform current velocity of 1.4 m/s ($Re = 3.23 \times 10^4$) and 1.7 m/s ($Re = 3.92 \times 10^4$). The simulation for V = 1.4 m/s and V = 1.7 m/s is run for 90000 and 80000 time steps respectively, to achieve steady state in crossflow and inline direction and the dimensional time step obtained is 0.000193 seconds and 0.000158 seconds respectively. The VIV simulation results are compared with Test 2120 and Test 2150 from NDP experiments which were released on MIT VIV data repository. Fig. 10 and Fig. 11 represent the snapshots of VIV evolution in the riser with time for both the test cases (Test 2120 and Test 2150). The riser starts from a stationary state and gradually starts deflecting in inline direction. After a certain number of time steps the crossflow time history reaches a steady state. The riser continues to deflect in inline direction until a stable steady state position is reached. Only crossflow VIV analysis is presented in this section as the inline VIV wasn't able to reach a steady state and more number of iterations were not possible due to time limitations.

Figure 10. Snapshots of VIV evolution for V = 1.4 m/s at a) 0.193 secs b) 3.18 secs and c) 5.4 secs

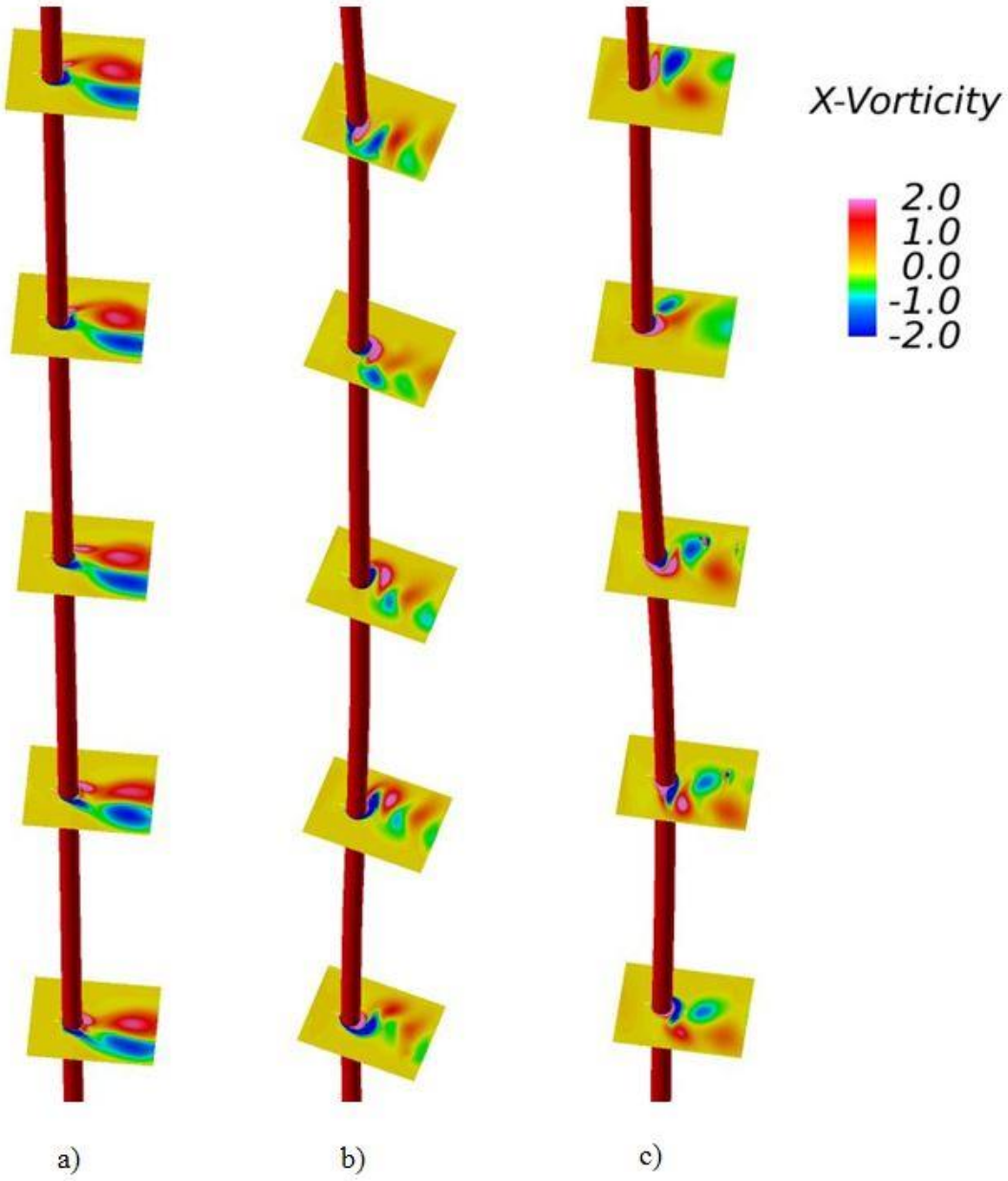

Figure 11. Snapshots of VIV evolution for V = 1.7 m/s at a) 0.193 secs b) 3.18 secs and c) 5.4 secs

Both the tests use a set of 24 crossflow strain signals to extract strain time histories. In this paper, a method developed by Trim et al. (2005) to utilize strain and

acceleration time signals to reconstruct the displacement time series is used. Fig. 12 and Fig. 13 show the comparison of crossflow RMS data between the CFD simulation and NDP experiments for Test 2120 and Test 2150 respectively. A very reasonable agreement can be seen between both time histories. A lot of scatter between the RMS comparison is observed in the latter case can be seen for higher velocities which needs further investigation.

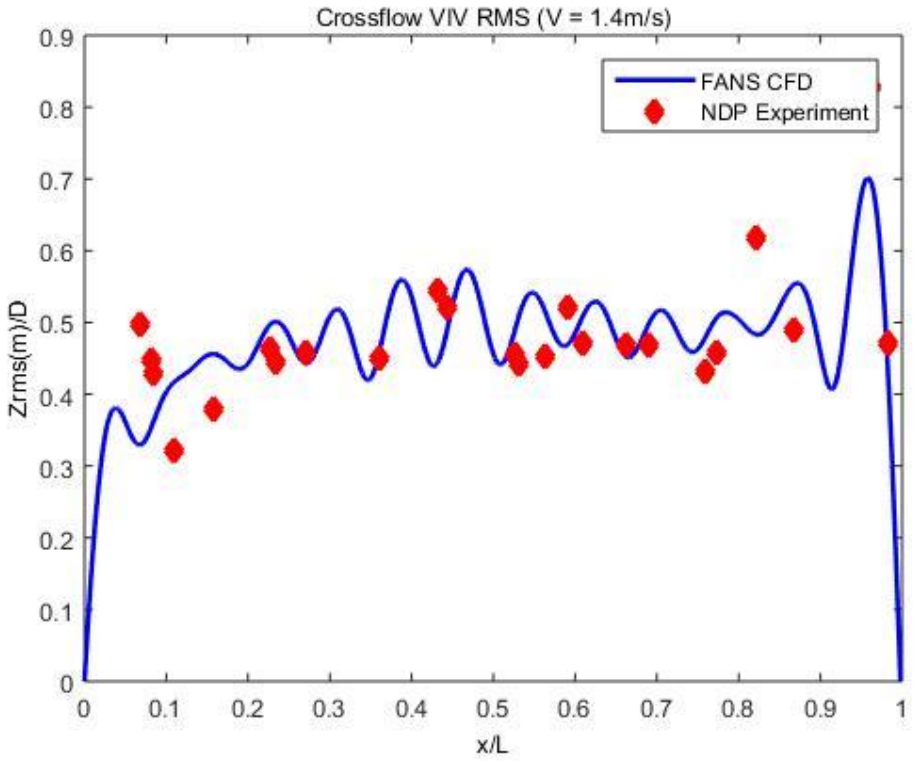

Figure 12. Crossflow RMS comparison between CFD simulation and NDP experiments (Test 2120)

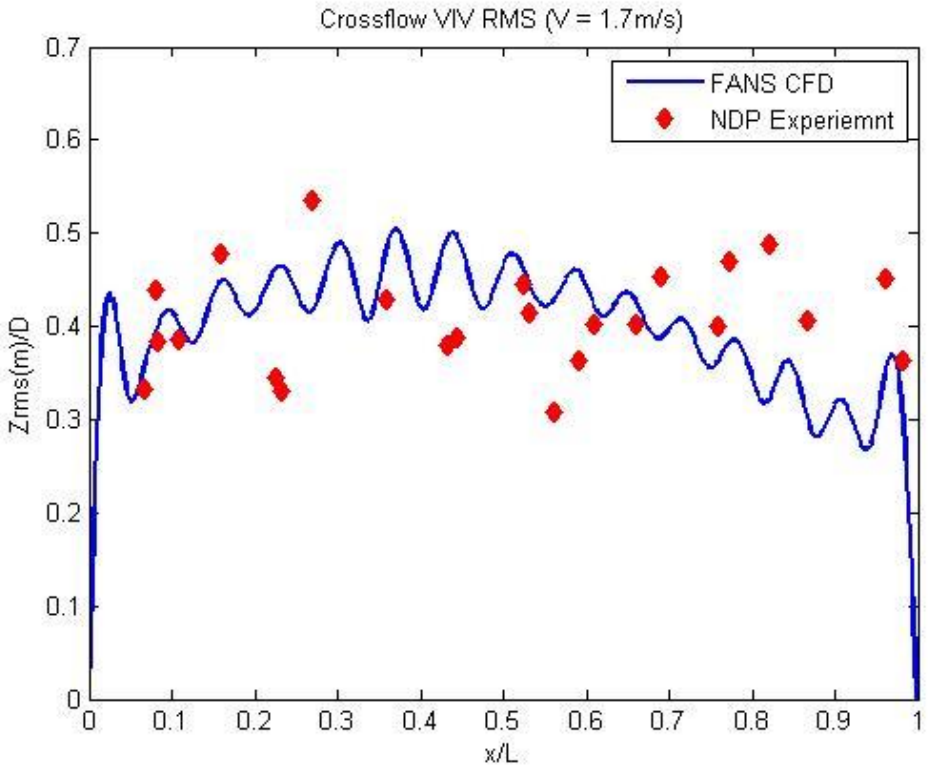

Figure 13. Crossflow RMS comparison between CFD simulation and NDP experiments (Test 2150**)**

A power spectral density (PSD) analysis is conducted and plotted in Fig. 14 - Fig. 17. The crossflow peak frequency occurs at ~ 8.9 Hz in test 2120 whereas the peak frequency occurring in CFD simulation is around 10.5 Hz for the test 2120. In case 2150 the peak frequency occurs at 9.64 Hz in experiments and 11.5 Hz in CFD simulations. One reason for this discrepancy can be attributed to tension variation in experiments. The riser pipe was subjected to a fluctuating tension of 4 kN ~ 6 kN during the tests whereas the CFD simulation used a constant tension of 5 kN.

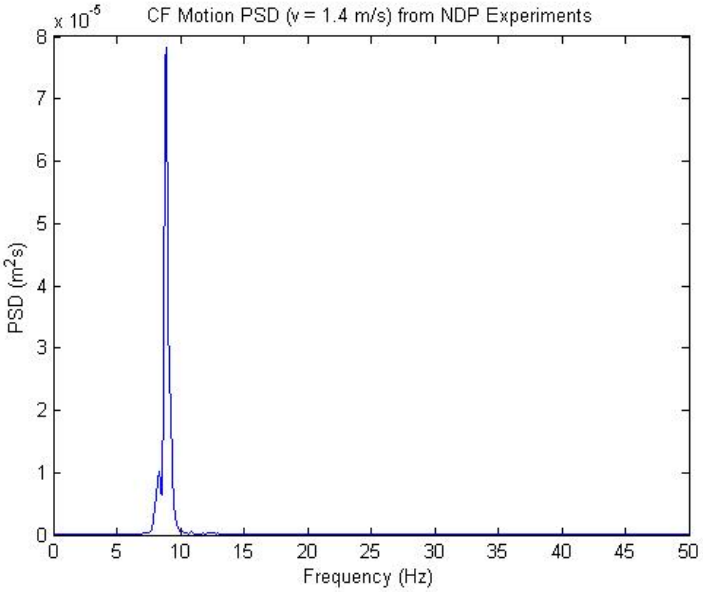

Figure 14. Riser crossflow PSD analysis at x/L = 0.52 from test 2120 (V = 1.4 m/s**)**

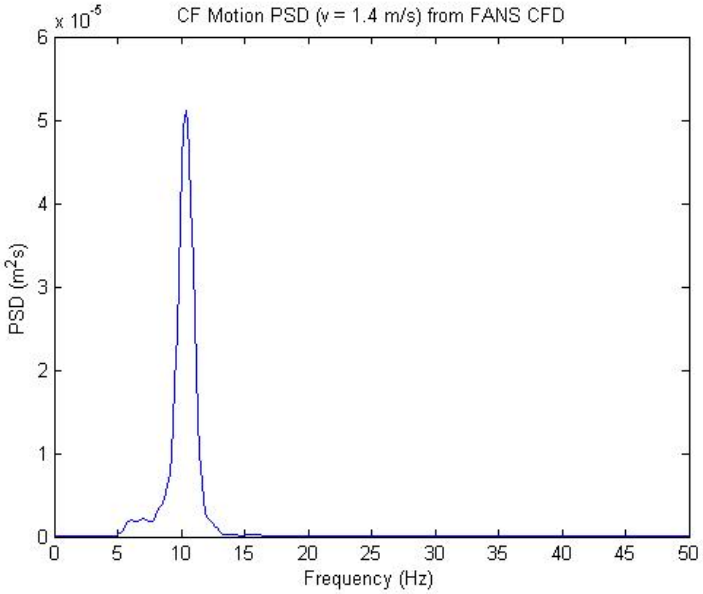

Figure 15. Riser crossflow PSD analysis at x/L = 0.52 from FANS CFD simulation (V = 1.4 m/s)

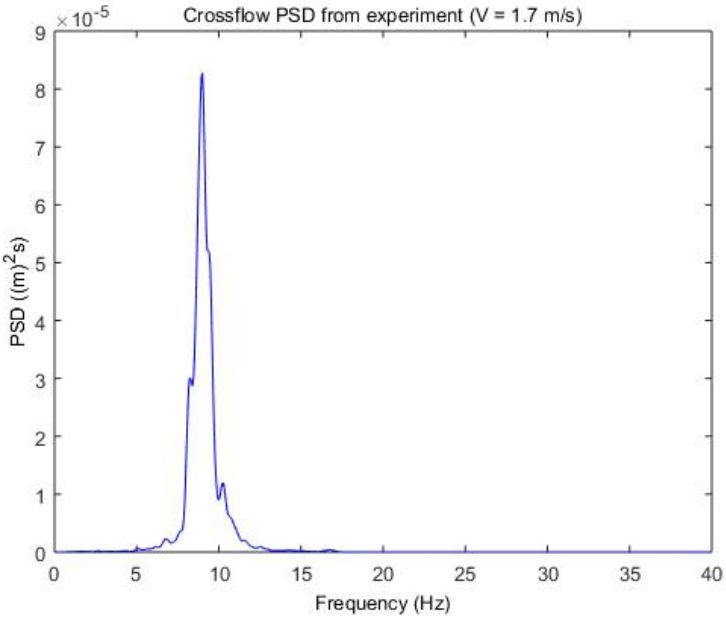

Figure 16. Riser crossflow PSD analysis at x/L = 0.52 from test 2150 (V = 1.7 m/s)

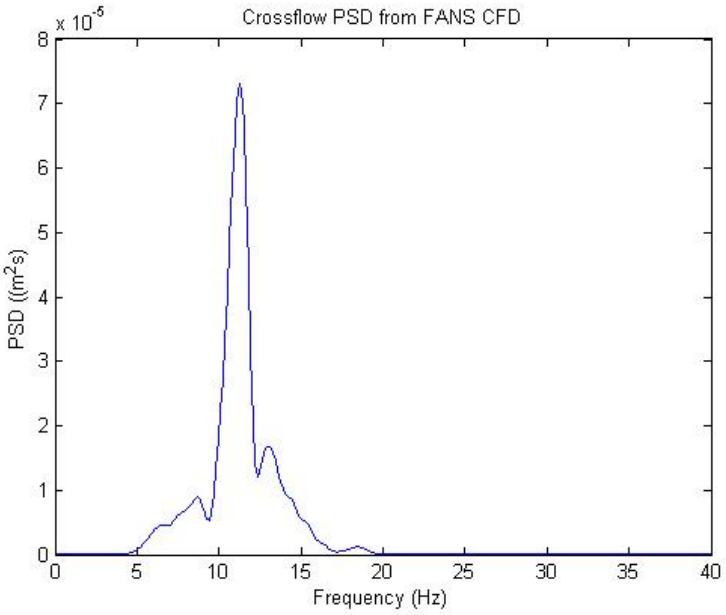

Figure 17. Riser crossflow PSD analysis at x/L = 0.52 from FANS CFD simulation (V = 1.7 m/s)

Fig. 18 and Fig. 19 depict the motion trajectories from the NDP tests and the simulations for test 2120 respectively. The difference between the two plots is a result of insufficient inline steady state region. Similar results for test 2150 weren't plotted and there was no inline steady state data available from the simulations.

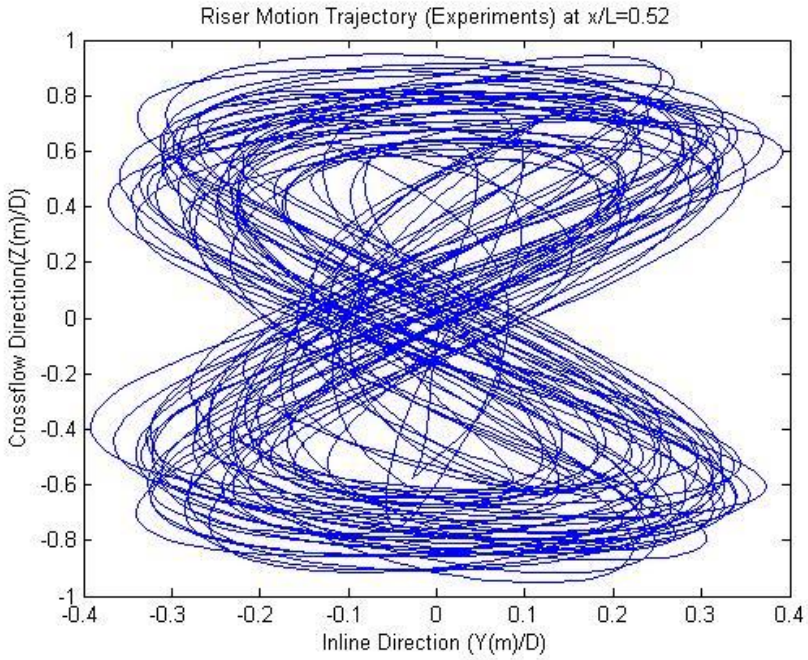

Figure 18. Riser crossflow trajectory from test 2120 (V = 1.4 m/s)

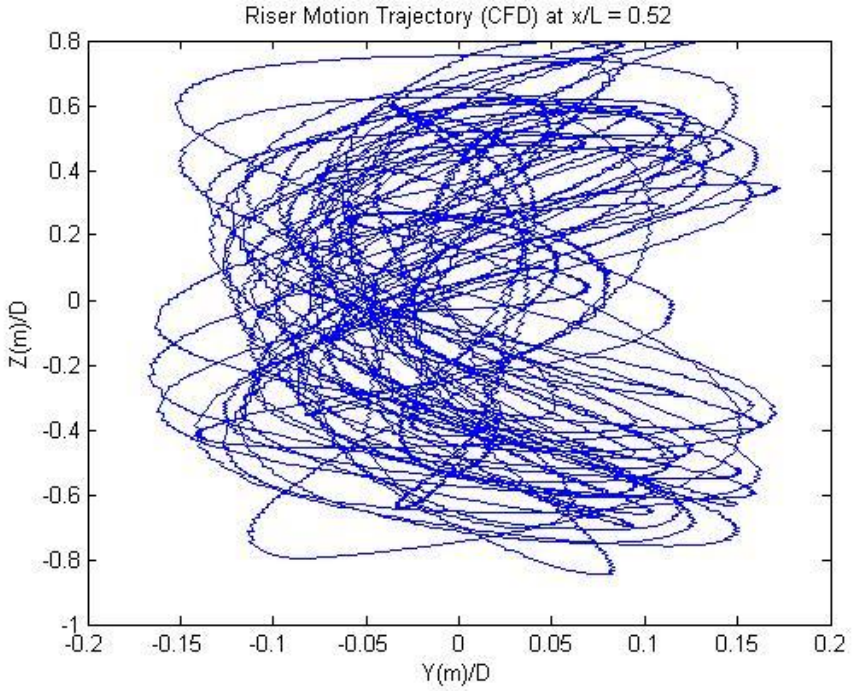

Figure 19. Riser crossflow trajectory from CFD simulation (V = 1.4 m/s)

Fig. 20 and Fig. 21 depict the crossflow fatigue comparison of the both tests from experiments and FANS CFD. The plots show very good comparison between the fatigue damages. Higher harmonics were removed for the fatigue analysis (Fig. 14 and Fig. 16) and only fundamental frequency fatigue damage was calculated from the experimental strain time series. This was done for accurate comparison with fatigue damage predicted by CFD simulation as the simulations weren't able to predict the higher harmonics (Fig. 15 and Fig. 17). From Thorsen et al. (2015), it can be shown that the maximum fatigue damage with higher harmonics for V = 1.4 m/s is small compared to the total fatigue damage and hence the CFD results are reliable. For V = 1.7 m/s the fatigue damage from higher harmonics is quite significant and further analysis is needed to resolve this issue.

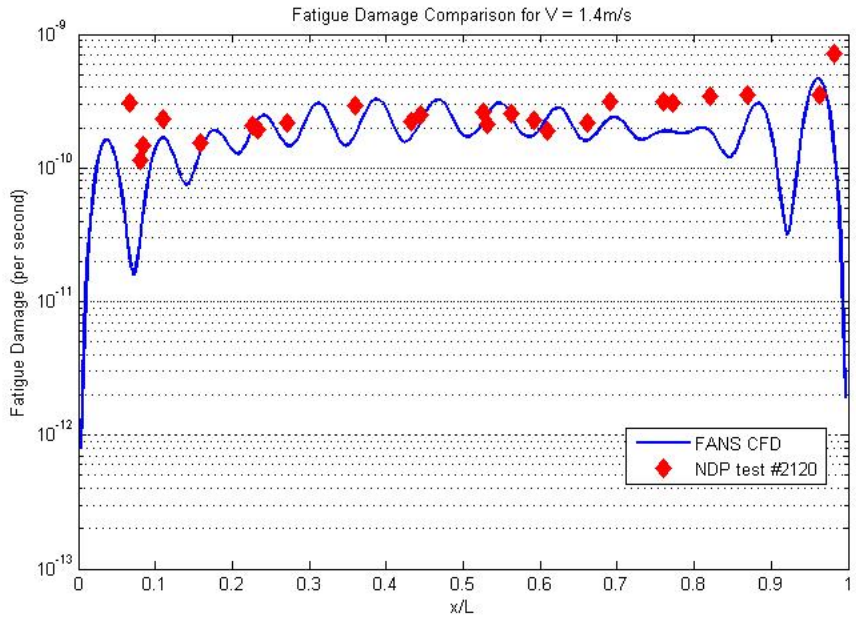

Figure 20. Riser crossflow VIV fatigue damage comparison (V = 1.4 m/s)

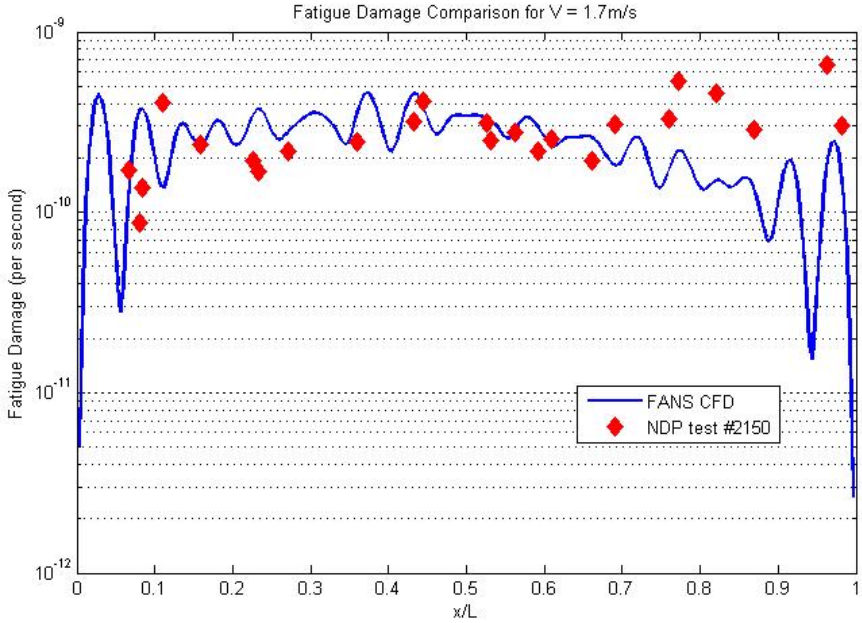

Figure 21. Riser crossflow VIV fatigue damage comparison (V = 1.7 m/s)

In this study two more uniform velocities (V = 0.3 m/s and U = 0.7m/s) were also analyzed to compare the statistics with experimental investigation of NDP experiments by Trim et al. (2005). A plot of crossflow RMS motion is studied and plotted in Fig. 22. The plots show increasing sinusoidal fluctuations of the RMS values with increasing current velocities. As the current velocity increases, the mode at which the riser vibrates goes higher.

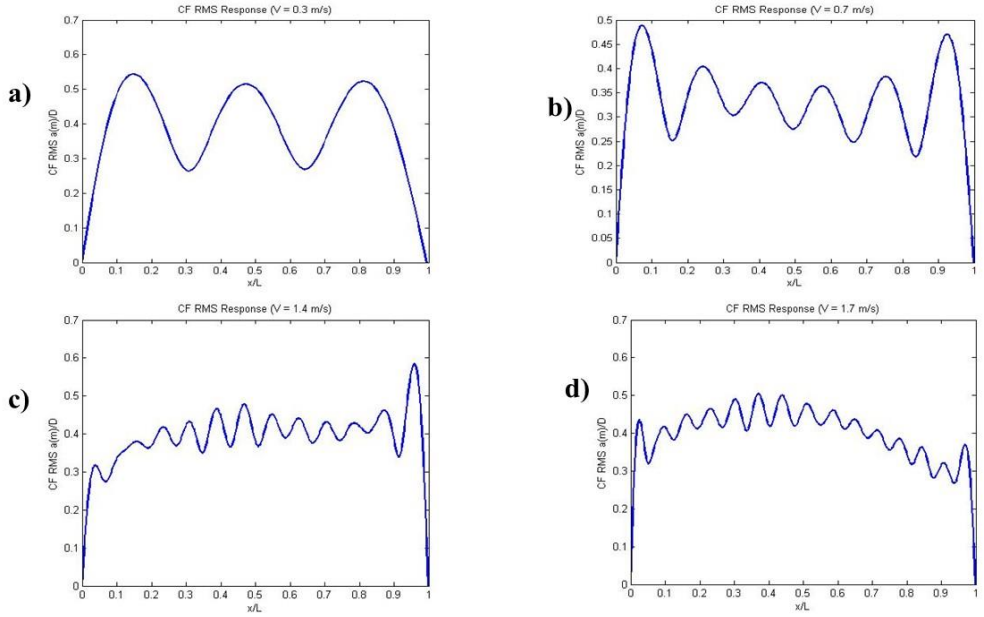

Figure 22. Riser crossflow VIV RMS for a) 0.3 m/s b) 0.7 m/s c) 1.4 m/s and d) 1.7 m/s

A modal decomposition of all the four velocities is shown in Fig. 23. A least square method is used for this analysis. Riser crossflow displacements are assumed to be a summation of sinusoidal modes and their model weights as presented in Eq. (6)

$$Z(x,\mathrm{t}) = \sum_{i=1}^{N} W_i(t)\xi_i(x) \tag{6}$$

where $Z(x,t)$ represents the crossflow motion, $W_i(t)$ presents the modal weight for each mode i and $\xi_i(t)$ is the sinusoidal mode shape as given in Eq. (7).

$$\xi_i = \sin\left(\frac{i\pi x}{L}\right) \tag{7}$$

The least square method is used to extract the modal weight $W_i(t)$ is given in Eq. (8)

$$W(t) = (\xi^T \xi)^{-1} \xi^T Z(x,t) \tag{8}$$

The 3rd mode is dominant in U =0.3 m/s, 6th Mode is the dominant mode in U = 0.7m/s. Similarly, 12th Mode and 15th Mode are dominant in U = 1.4m/s and 1.7 m/s respectively. Fig. 24 shows the crossflow power spectral density functions and the peak frequency at which the riser vibrates. Modal weights for dominant modes steadily decreases with increasing velocity as more and more energy gets distributed over wider range of frequencies as shown in the plots.

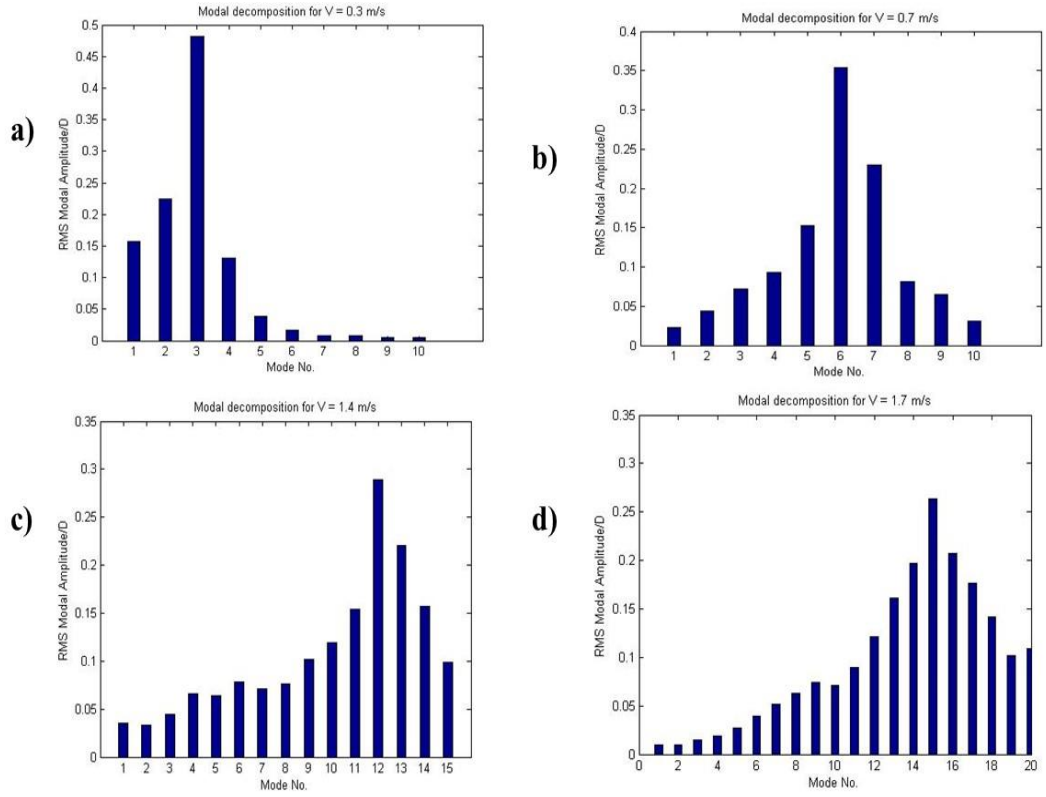

Figure 23. Crossflow modal decomposition for a) 0.3 m/s b) 0.7 m/s c) 1.4 m/s and d) 1.7 m/s

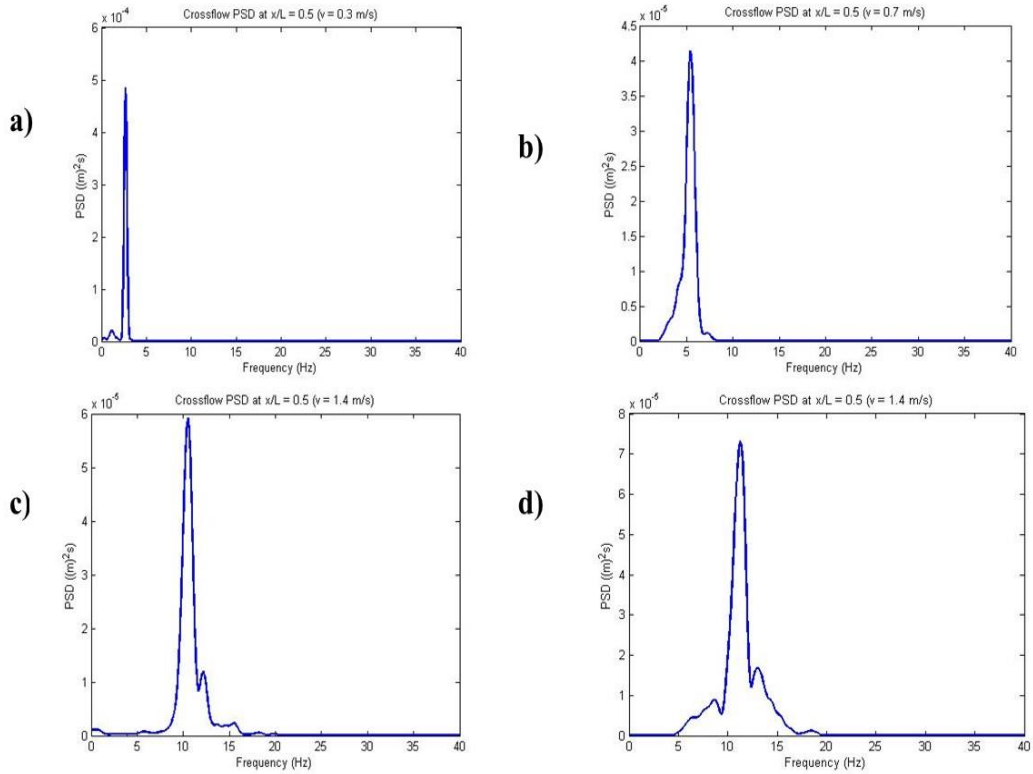

Figure 24. Crossflow PSD analysis for a) 0.3 m/s b) 0.7 m/s c) 1.4 m/s and d) 1.7 m/s

A comparison with published data from NDP Experiments by Trim et al. (2005) is plotted in Fig. 25 – Fig. 28. Fig. 25 depicts the comparison of mean Crossflow RMS with experimental data. A very good comparison can be seen at low velocities. At higher velocities, a larger distribution of crossflow response over wider range of frequencies and modes is observed as shown in Fig. 23 and Fig. 24 which causes the RMS values to deviate from experiments. Fig. 26 also predicts similar behavior with modes accurately predicted at low velocities. Further analysis is needed to understand the effect of higher velocities in prediction of higher modes by CFD. Fig. 27 shows the peak frequencies observed in CFD simulations and its comparison with the test. The trend of over-

predicting the values for higher velocities can also be seen in this figure. Fig. 28 shows the fatigue damage observed in the CFD simulations. As mentioned above the strain signals from experiments were filtered for higher harmonics and Fig. 28 shows the damage rate associated with only the dominant mode. It was shown in Thorsen et al. (2015) that the higher harmonics are important in prediction of the fatigue damage. In CFD simulations the higher harmonics were not predicted due to coarse resolutions which led to concentration of strain energy only at fundamental frequencies. This caused an apparent increase in fatigue damage with fundamental frequency response by CFD which can be seen in Fig. 28 for U = 0.3 m/s and U = 0.7 m/s. The fatigue damage rate is smaller for U = 1.4 m/s and U = 1.7 m/s compared to published data which might be attributed to Fatigue Convergence. Huang, Chen and Chen (2008) studied the dependence of the fatigue damage on the number of iterations and specified the minimum iterations required for convergence for V = 0.4 m/s. Higher velocities require significantly more number of iterations to achieve converge. This was not possible due to time limitations.

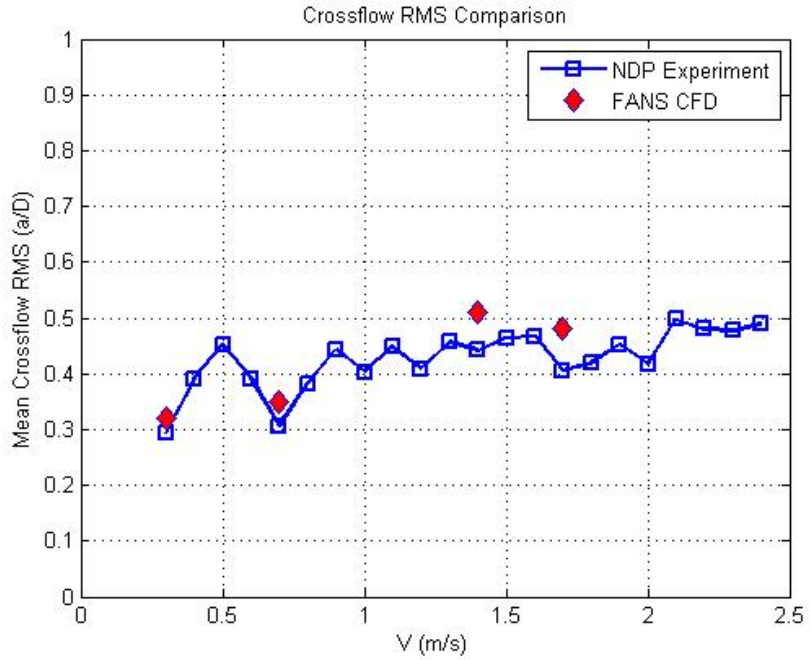

Figure 25. Mean riser crossflow RMS comparison between CFD simulation and experiments

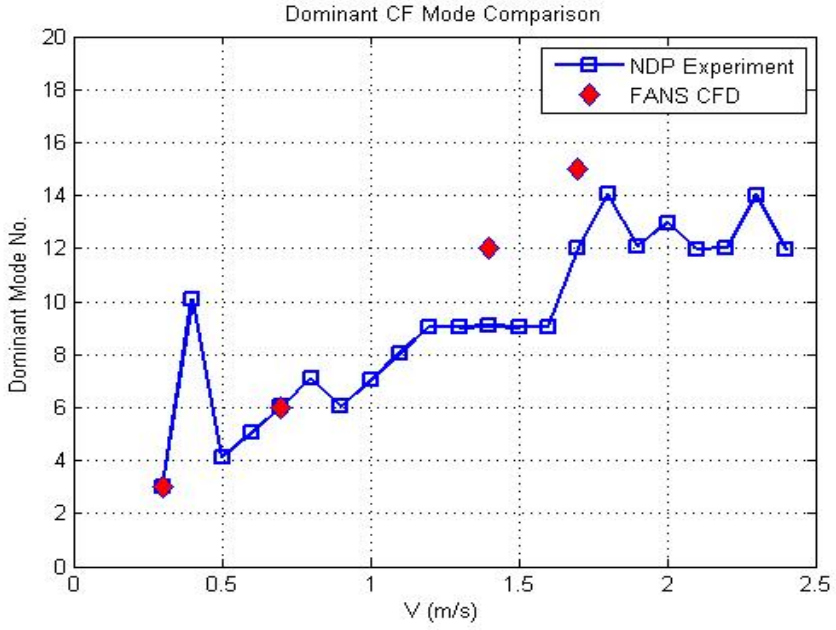

Figure 26. Dominant mode distribution between CFD simulation and experiments

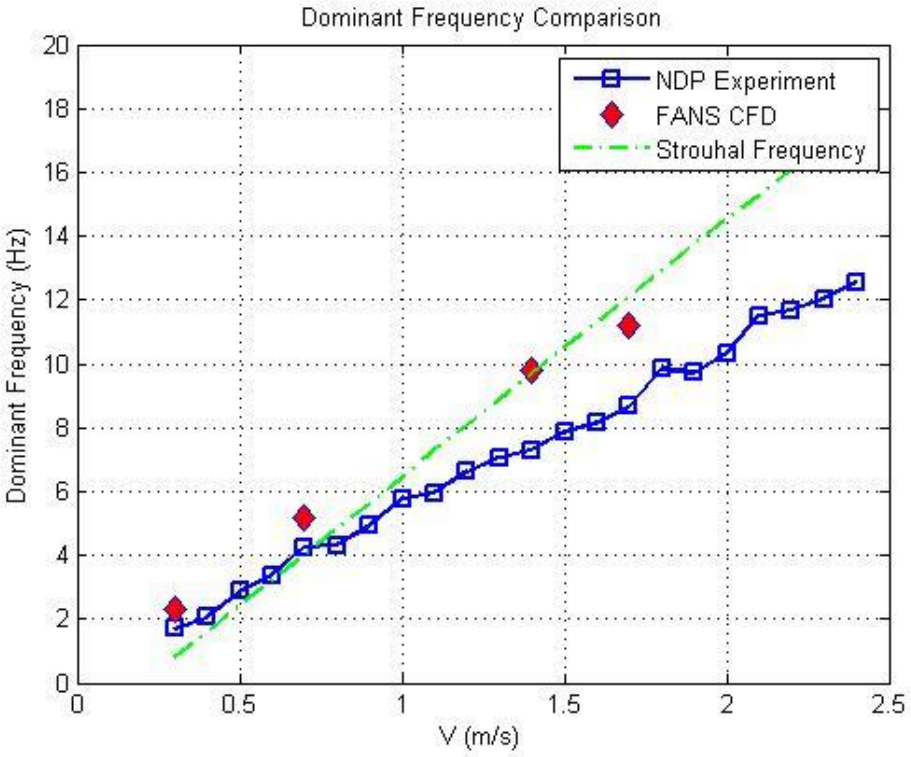

Figure 27. Dominant frequency distribution between CFD simulation and experiments

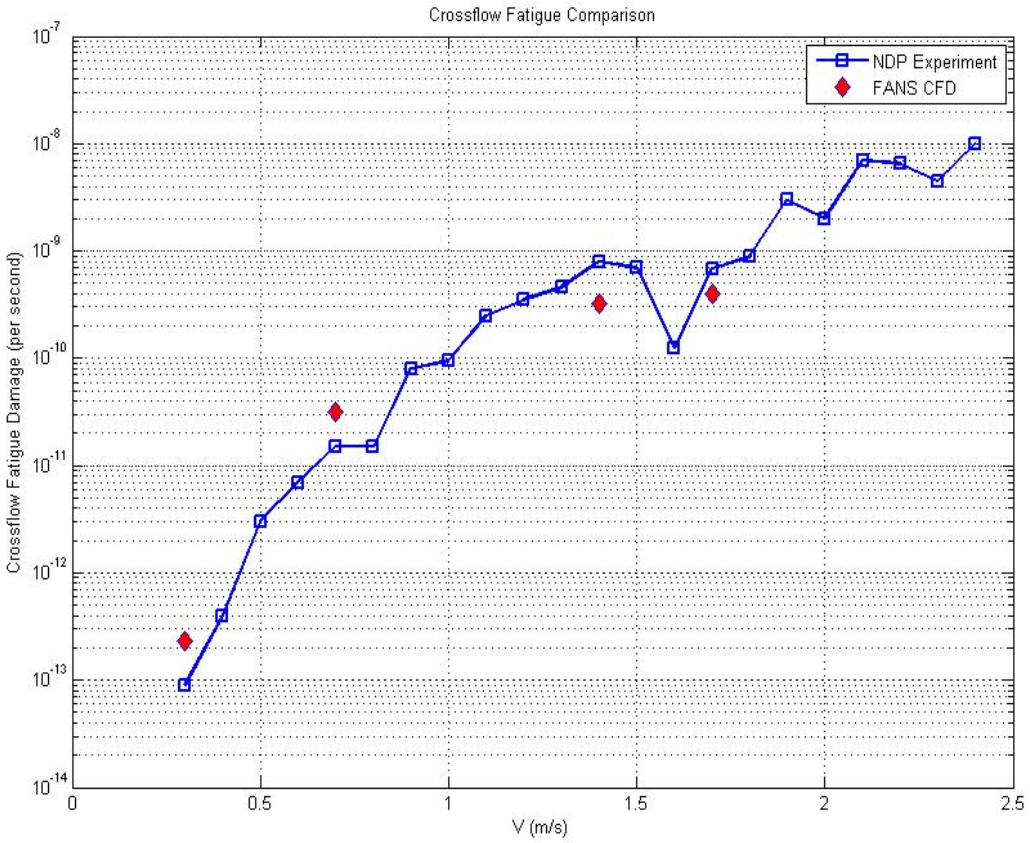

Figure 28. Maximum crossflow damage rate comparison between CFD simulation and experiments

CHAPTER IV

RISER IN SHEARED CURRENT

A riser of length 38 m and outer diameter of 0.027 m is placed in a linearly sheared flow to study VIV response and extract fatigue damage induced by shear current. The riser properties are similar to that used in Chapter III and are obtained from NDP (2003) experiments. In this chapter, a detailed analysis of the riser with max sheared velocity of 0.7 m/s is presented including motion RMS comparisons, power spectral density analysis, modal decomposition and fatigue damage plots.

Experimental Setup

The experimental setup is similar to the one presented in Chapter III for the uniform flow. The only difference being that the gondola traverses a circular arc to generate a linearly sheared current profile. The orientation between the clump weight and the riser is maintained at a fixed angle by turning the complete test rig at the end attached to gondola. A computer was used to regulate the turn and a 2-3 cm accuracy was achieved. Fig. 29 describes the model test setup for sheared current case.

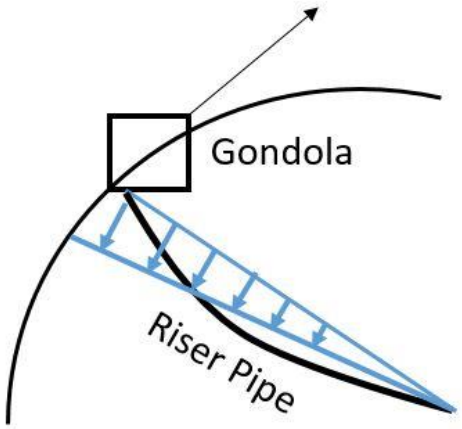

Figure 29. Experimental setup for sheared current used in NDP expts (Trim et al., 2005)

Numerical Simulation Results

The riser is simulated with a riser grid of 223860 (30 X 182 X 41) elements and a wake grid of 609030 (30 X 201 X 101) grid elements. A shear current profile is specified at each grid point in both the grids with a maximum velocity of 0.7 m/s at one end. This end was selected randomly as the riser is horizontally positioned and the tension gradient is negligible. NDP released two datasets from their experiments with linearly sheared current profiles in MIT VIV Data Repository. In this study test 2350 with max velocity of 0.7 m/s was used to benchmark the FANS CFD solver and compare the numerical results. A simulation is run for 40000 time steps achieving a steady state region in both crossflow and inline direction.

FANS CFD solver uses a non-dimensional sheared current profile at the inlet. The inlet boundary uses this current profile as the "prescribed" boundary condition. A dimensional time step of 0.000386 is used in this analysis with a Reynolds Number of $1.62 \text{ X } 10^4$. The initially straight riser deflects in the inline direction at the beginning and continues deflecting downstream till the fluid forces acting on the riser and the structural restoring forces from the riser reach equilibrium.

As mentioned previously, VIV analysis for both inline and crossflow motions is presented in this section. It is found that the inline motion takes a longer time to reach steady state in longer risers and higher current velocities. Nevertheless, the inline comparisons demonstrated in the following figures are very encouraging. A Root Mean Square (RMS) comparison of inline and crossflow motions is presented in Fig. 30 and Fig. 31.

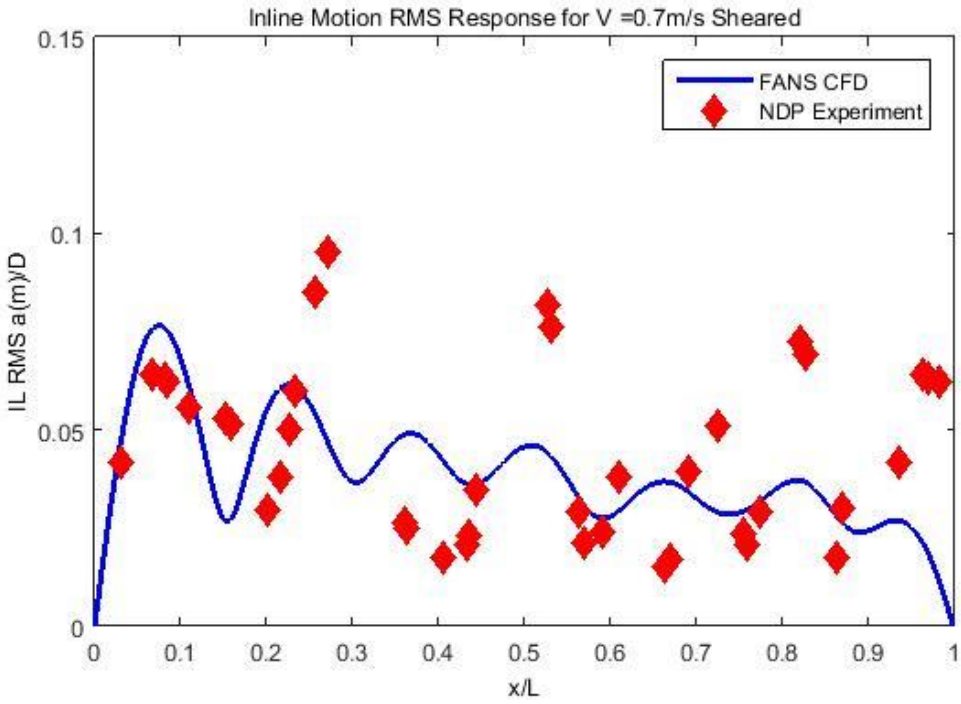

Figure 30. Inline RMS motion comparison between CFD simulation and test 2350

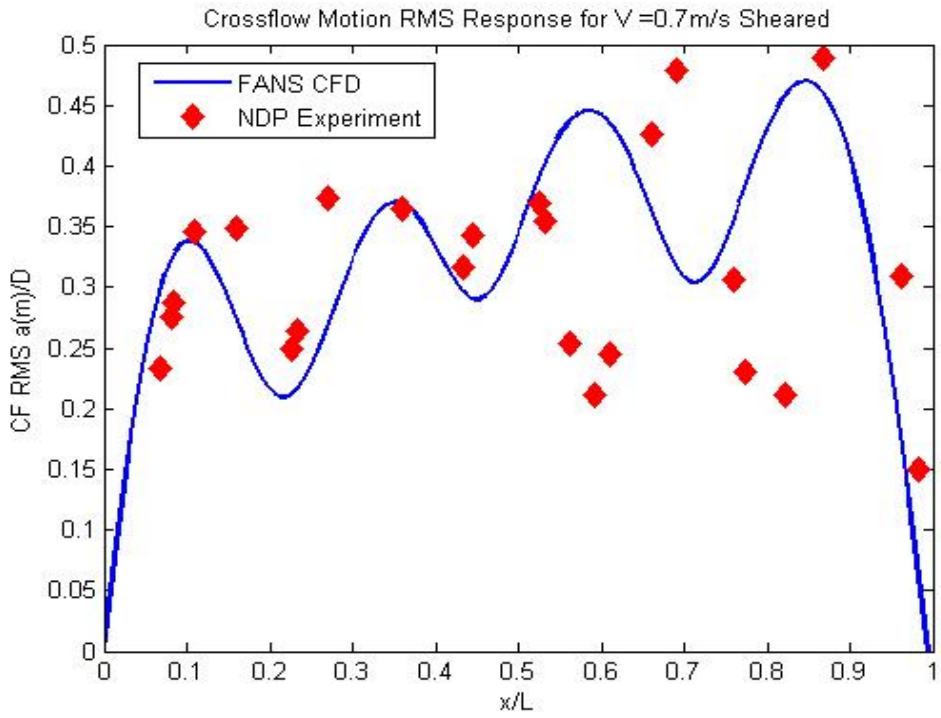

Figure 31. Crossflow RMS motion comparison between CFD simulation and test 2350

The motion comparisons show a very good agreement between the simulation results and NDP Experiment. The maximum RMS value for Crossflow Motion Response is 0.46D from the simulations and 0.49D from the experiments. This maximum response occurs at the end of the riser in both the cases where the largest shear current values are observed. A significant difference between the values from numerical simulation and field tests can be seen in Fig. 30. In the simulations inline motion was superimposed with slow drift motion of the riser at lower frequency which was filtered out for analysis. This drift motion drained energy content from the high frequency inline motion which was therefore reduced in amplitude. Advanced filtering techniques using signal processing and high pass filters can be used to solve this problem.

A Power Spectral density analysis is performed on inline motion of the riser and the results are presented in Fig. 32 and Fig. 33. The peak frequency occurs at 5.5 Hz in the simulations and occurs at 6.7 Hz in experiments for inline motion. The significant difference between the peak frequencies could be due to interference from the low frequency mean drift component. Crossflow PSDs are presented in Fig. 34 and Fig. 35 where the peaks frequencies are occurring approximately at the same frequency of 3.6 Hz.

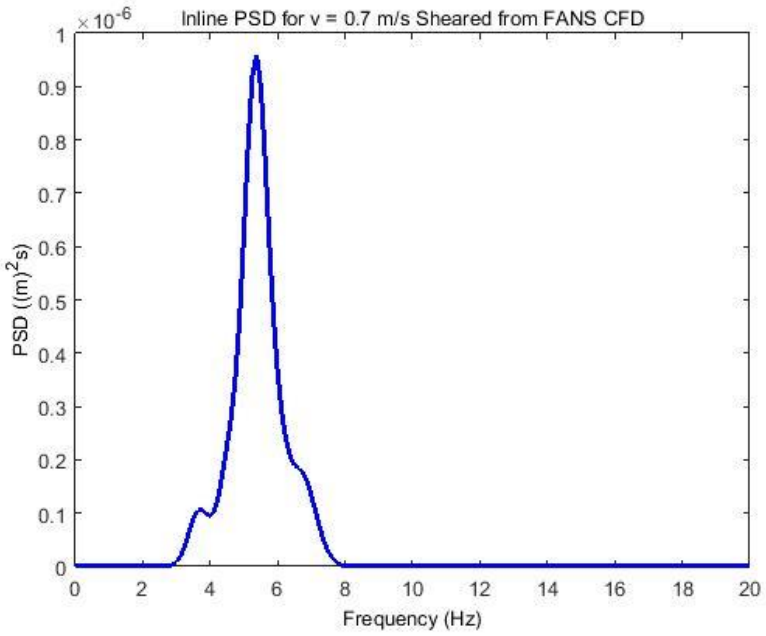

Figure 32. Inline PSD analysis from CFD simulation (low frequencies filtered out)

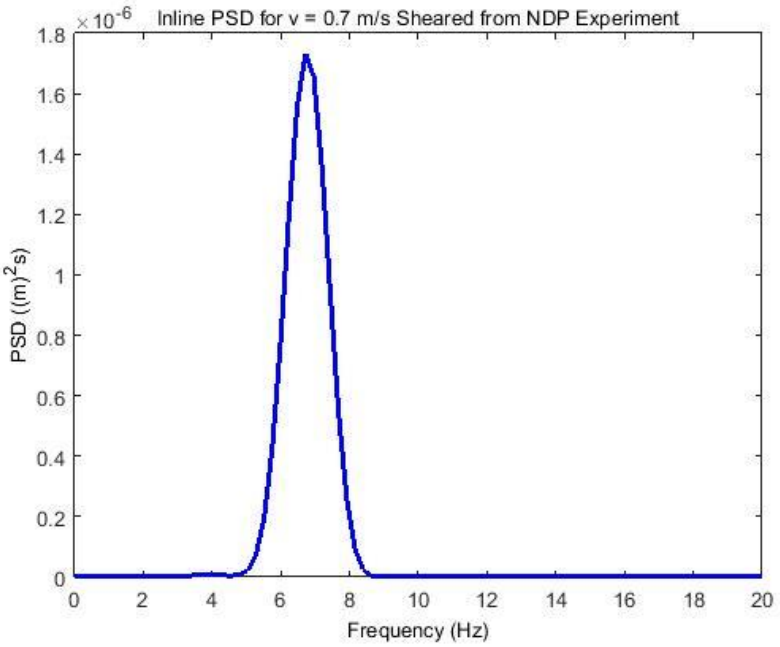

Figure 33. Inline PSD analysis from test 2350 of NDP experiments (3x and higher components filtered out)

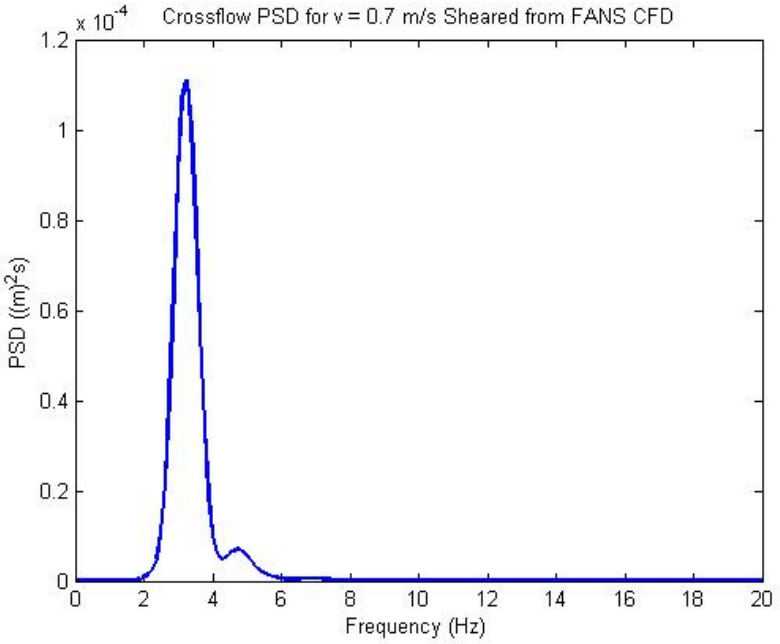

Figure 34. Crossflow PSD analysis from CFD simulation

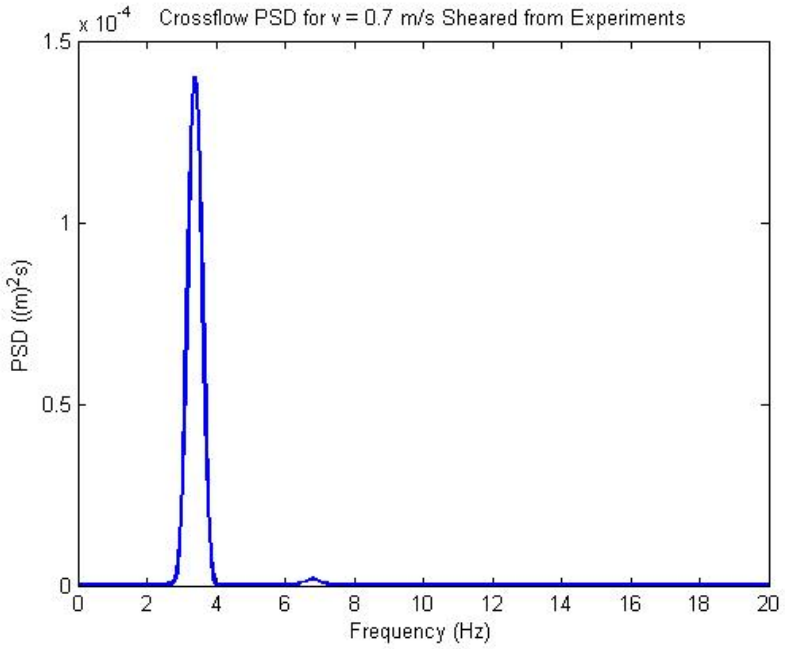

Figure 35. Crossflow PSD analysis from test 2350 of NDP experiments (3x components filtered out)

A modal decomposition approach used in the previous chapter has been applied to obtain the modal weights associated with the inline and crossflow motions as presented in Fig. 36, Fig. 37, Fig. 38 and Fig. 39. 7th Mode is dominant in inline VIV from the numerical results whereas inline VIV from NDP experiments is dominated by 9th Mode. As seen in Fig. 38 and Fig. 39, 4th Mode is dominant in crossflow direction from CFD simulation and 5th Mode is dominant in the crossflow motion from field tests. The differences between the peak frequencies and dominant modes in FANS CFD and NDP experiments can be due to the tension variations experienced while running the model tests. In experiments the tension varied between 4 kN – 6kN whereas it was kept

at a constant value of 5 kN in CFD simulations. Two interesting observations are made based on the modal analysis:

1) The inline modal analysis from experiments indicates a higher value of fundamental mode acting on the riser which might have been a result of gravity acting on the system.
2) Crossflow modes obtained from FANS CFD show a distribution of energy in 3rd and 5th modes and thereby lowering the modal value associated with 4th Mode to 0.32D when compared to 0.5D obtained from experiments which could be a result of added mass variations due to rotation of the riser.

As discussed earlier, inline motion is very strongly influenced by lower modes and it is seen that the mean value for equilibrium between the fluid forces and riser structural forces increases as a square of velocity (Drag Force $\propto$ velocity^2). This makes it very difficult to extract inline motion data from the riser displacement in the inflow direction. To add to the complexity of the problem, the riser deflection induced by the low frequency motions causes the riser to disturb its own VIV pattern. As a result inline VIV analysis becomes increasingly difficult with increasing velocity and riser length. Further investigation is needed to eliminate the impact of riser flexibility on inline motion and accurately extract the VIV data.

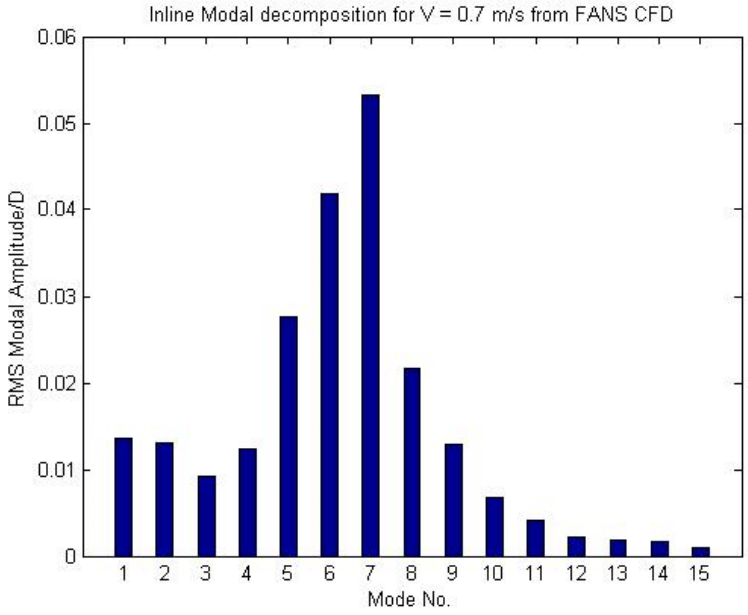

Figure 36. Inline modal decomposition from CFD simulation (low frequencies filtered out)

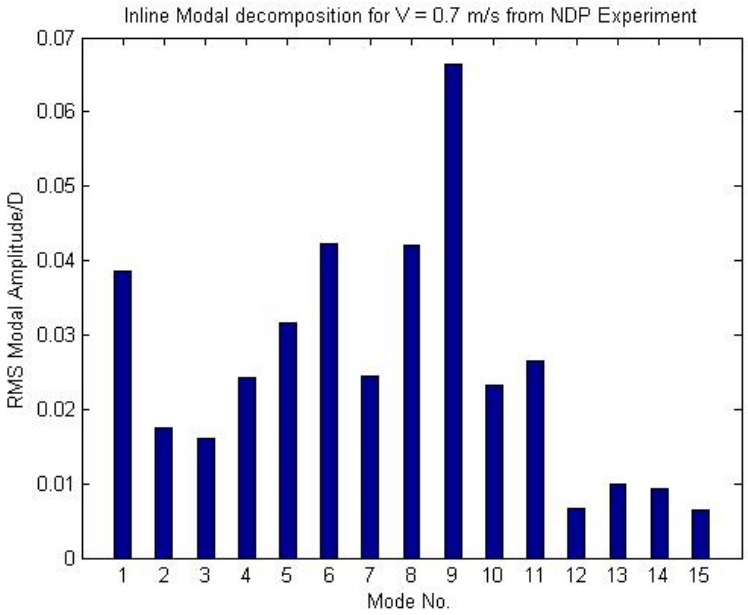

Figure 37. Inline modal decomposition from test 2350 of NDP experiments (3x components filtered out)

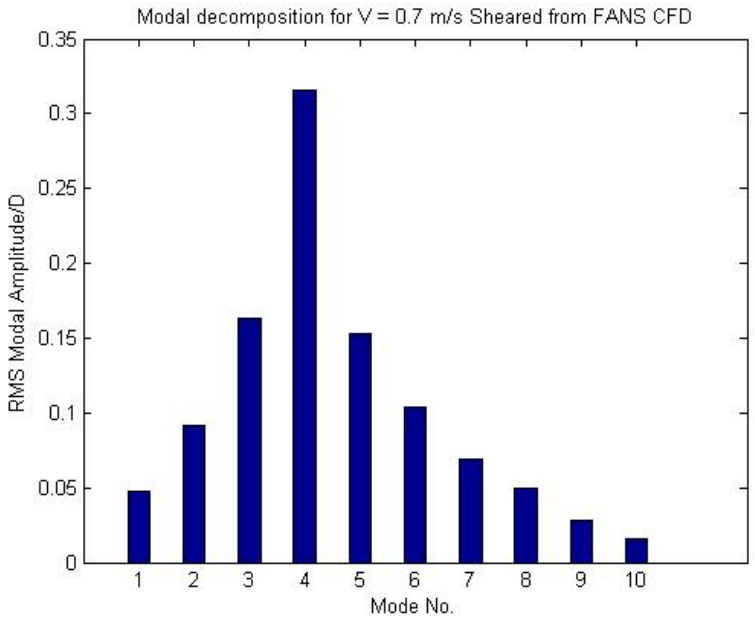

Figure 38. Crossflow modal decomposition from CFD simulation

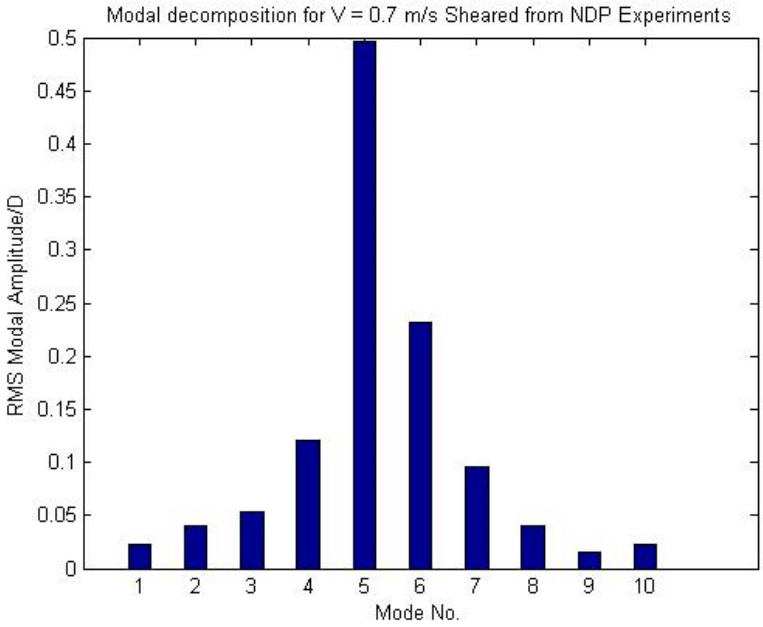

Figure 39. Crossflow modal decomposition from test 2350 of NDP experiments (3x components filtered out)

Fig. 40 depicts the vortex shedding snapshots at t= 0.386 seconds, t= 3.86 seconds and t = 7.71 seconds. The vortex contours generated at the aft of the riser clearly follow a '2S' pattern.

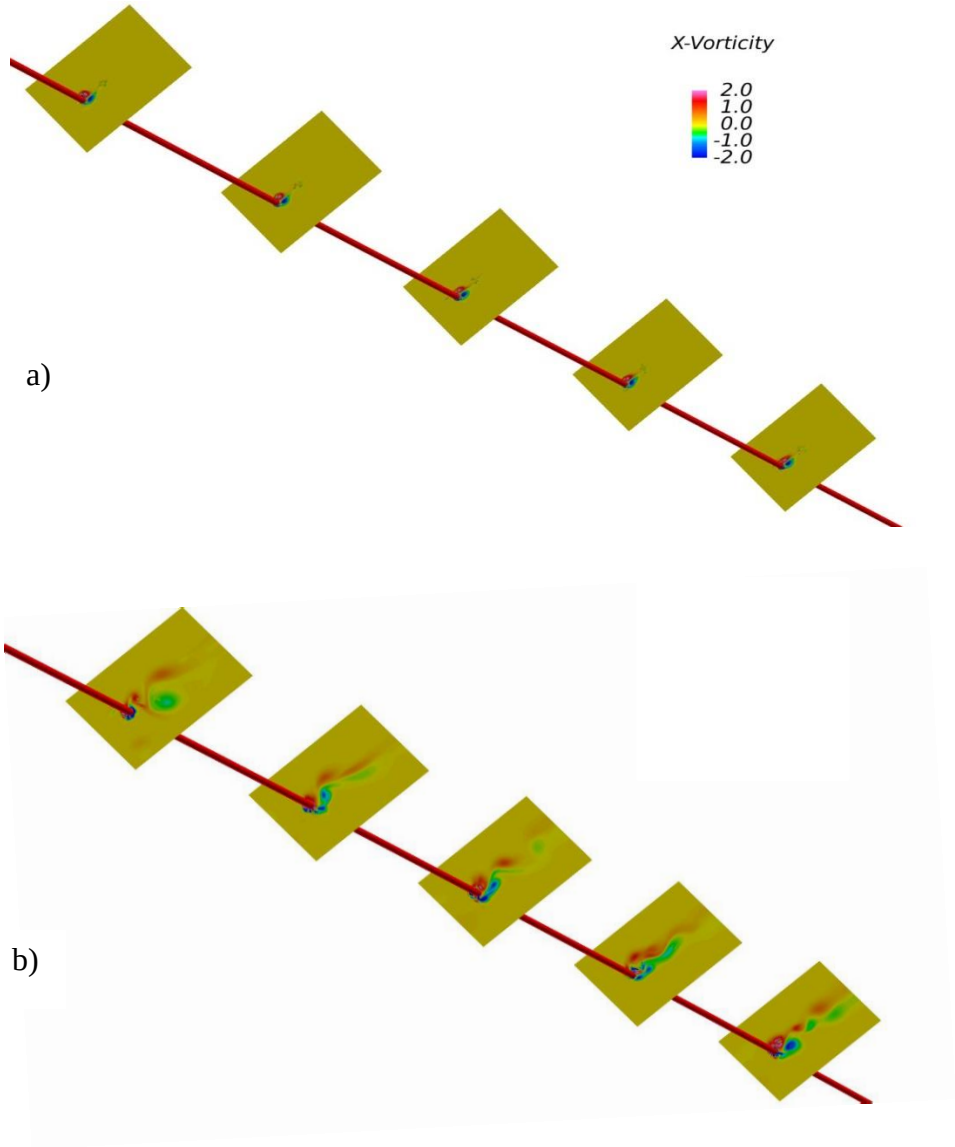

Figure 40. VIV evolution for riser in sheared current at a) t = 0.386 seconds b) t = 3.86 seconds and c) t = 7.71 seconds

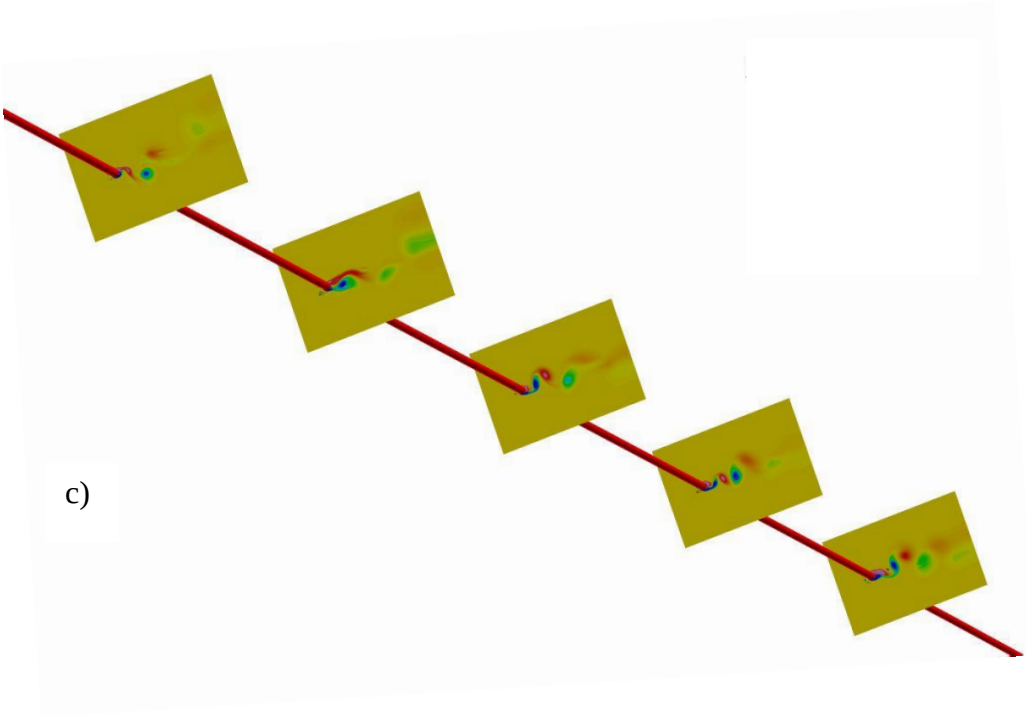

Figure 40. Continued

Fig. 41 and Fig. 42 show a comparison of the inline and crossflow VIV fatigue damage from the experiments and FANS CFD simulations. The crossflow fatigue from FANS CFD is in a reasonable agreement with the experiments results with comparatively low standard deviation. The inline fatigue damage on the other hand is relatively scattered with significant deviation between the CFD simulations and experiments. This is a direct consequence of the lower mode and peak frequency prediction due to the difficulties encountered while obtaining inline VIV responses. Nevertheless, FANS CFD is shown to reasonably predict both inline and crossflow VIV fatigue with reasonable accuracy. Maximum fatigue damage may not necessarily occur

at in inline and crossflow direction. Barrholm et al. (2006) have used a combination of crossflow and inline stresses by adding the components of stresses at 10^{o} intervals to obtain maximum fatigue damage at each cross-section. The inline and crossflow damages are shown to be smaller compared to the maximum fatigue damage of the combined stress components at certain axial positions. A 'fatigue surface' has been developed by Huang, Chen and Chen (2008) which presents the fatigue damages at each axial cross-section and every angular location. Therefore it is very important to not only consider damages occurring from inline and crossflow motions but their combination should also be analyzed to locate the critical fatigue locations.

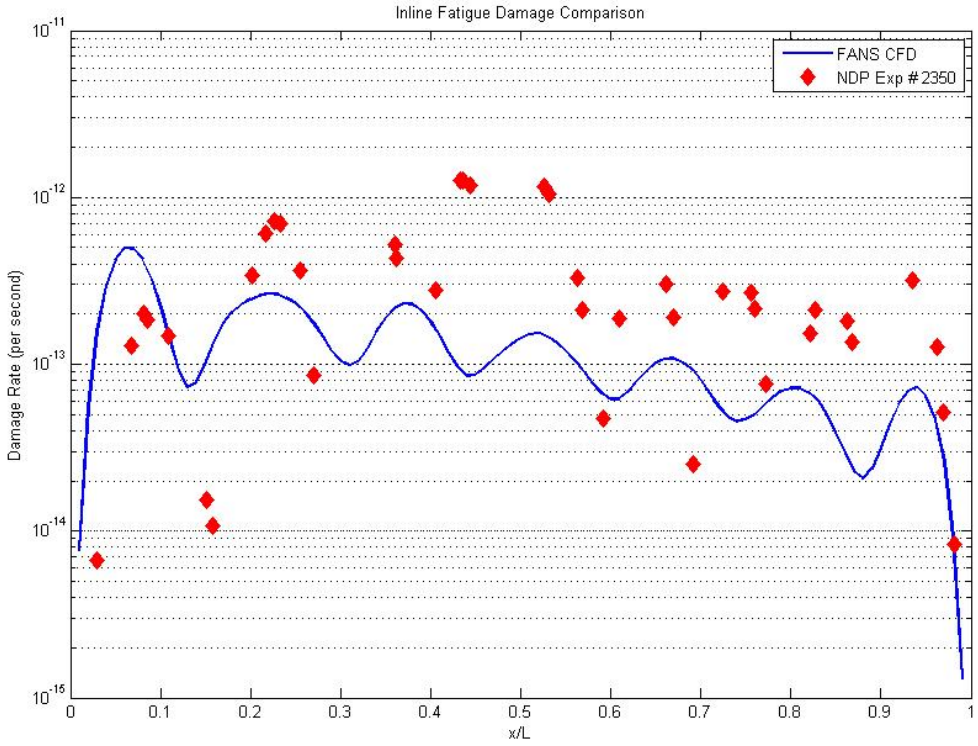

Figure 41. Inline fatigue damage comparison between CFD simulation and test 2350

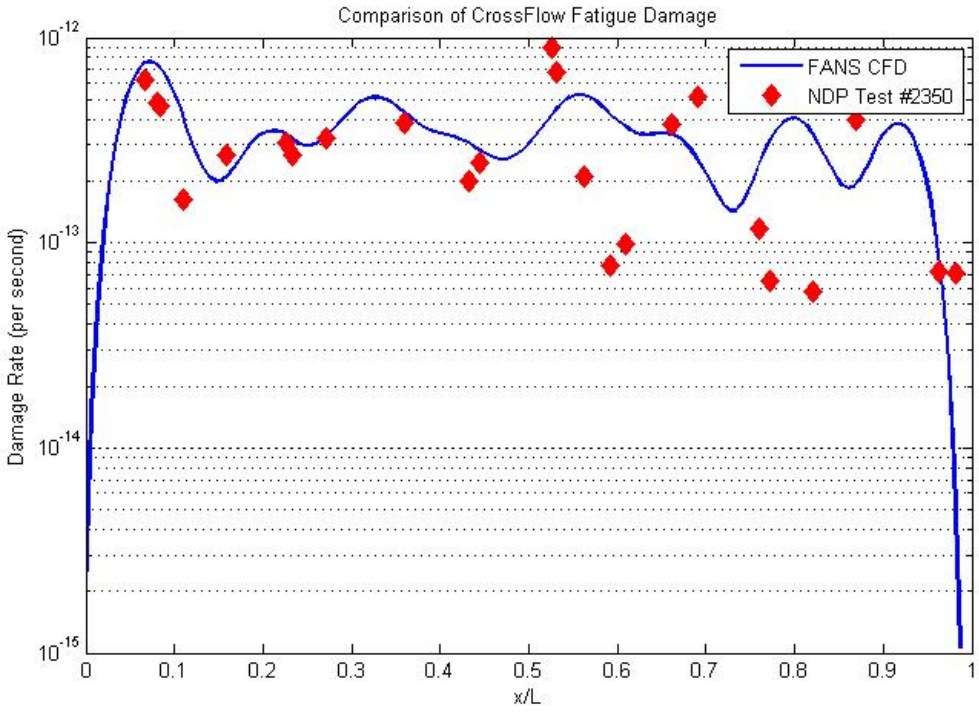

Figure 42. Crossflow fatigue damage comparison between CFD simulation and test 2350

CHAPTER V

RISER IN NON-UNIFOM CURRENT

Deepstar conducted a series of high mode VIV experiments in Gulf of Mexico in late 2006. These experiments used a very long riser of L/D ≈ 4200 in a highly nonlinear sheared (non – uniform) current. Owing to the extremely large length of the riser (500 ft), it was essential to have a finer resolution in axial direction to accurately simulate flow field around the riser. In this section, a riser with outer diameter of 0.0363 m and length 152.52 m has been used for comparisons of crossflow PSD analysis, RMS comparisons of strain time series and estimation of the crossflow fatigue damage along the riser.

Experimental Setup

In October 2006, a series of high mode number experiments were conducted on a research vessel near the coast of Miami in Gulf of Mexico and were sponsored by DeepStar. A set of three experimental test results for bare and straked risers were made available in MIT VIV data repository. In this analysis we have used the dataset "20061020174124" for a bare riser case. The riser pipe was towed with the help of the research vessel and a bottom weight of 3225 N was applied via a railroad wheel attached to the end of the pipe. The detailed experimental setup can be found in Fig. 43. The experiments were conducted to collect the data for high mode numbers (> 10) and were

designed to have a negligible response to bending stiffness. The recording instrumentation attached to the pipe contained fiber optic strain gauges and an Acoustic Doppler Current Profiler. The strain gauges were located inside optical fibers which were fixed at each quadrant of the riser. These fibers were installed at the spacing of 14 feet with a 7 feet spacing between strain gauges of adjacent fibers in each quadrant. The drag forces resulted in the pipe being slightly inclined to the oncoming current. Since the drag forces and lift forces for VIV calculation use a normal incident current velocity, the ADCP recordings were processed to generate the normal flow at each location on the riser. The riser properties are given in Table 2. Pinned boundary conditions were simulated in the experiments which are subsequently modeled in numerical simulations.

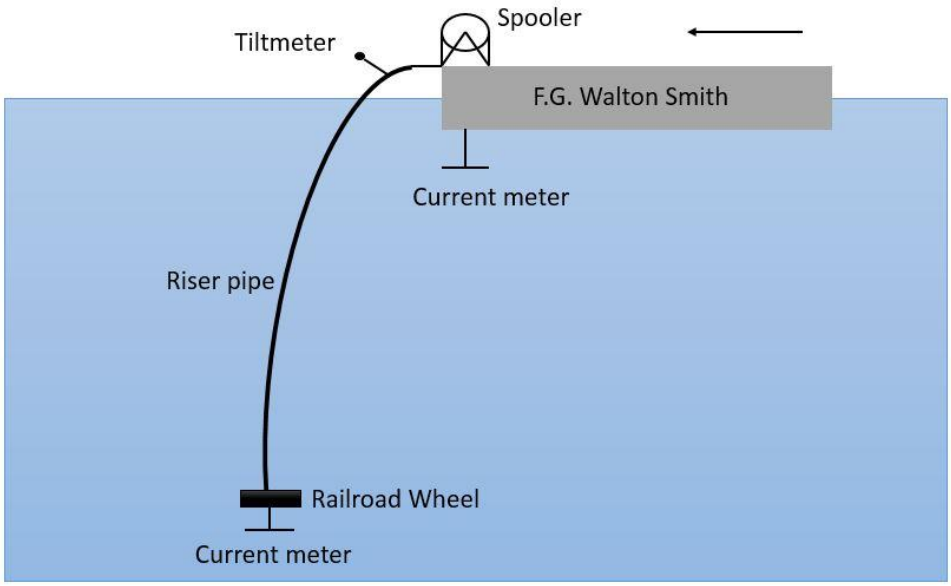

Figure 43. Field test setup for Miami2 2006 experiments (Vandiver et al., 2006)

Physical Property	Values
Length overall	152.524 m
Outer Diameter	0.0363 m
Inner Diameter	0.0249 m
Bending Stiffness, EI	613 Nm^2
Young Modulus for pipe, E	200 X 10^9 N/m^2
Axial stiffness, EA	3.322 X 10^6 N
Mass of the pipe (air filled)	0.760 kg/m
Mass of the pipe (water filled)	0.1972 kg/m
Effective tension	3225 N

Table 2. Riser properties from DeepStar Miami2 2006 experiments

Experimental Analysis

A highly non-linear sheared current profile was observed in the Miami2 filtered data and is presented in Fig. 44. There were several irregularities observed with the data recorded including sampling rate irregularities, strain over range and irregular stop and start signals. A major problem influencing VIV analysis was the twist observed in the riser during experiments. During manufacturing process, a residual twist was introduced which resulted in none of the fibers and strain gauges being perfectly aligned with the crossflow and inline direction. This can be seen via the power spectral density analysis

of the filtered strain time series. The extraction of true crossflow and true inline strain signals is essential for analyzing the fatigue life. A methodology presented in Vandiver et al. (2007) was used to decouple the crossflow and inline components from the recorded signals. The crossflow and inline power spectral density functions at each sensor locations are rotated from 0 to 180 degrees. The angles corresponding to maximum energy concentrated at the 1x and 3x frequencies are used to determine the true crossflow strain time series. Similarly, the angles with maximum PSD function values in 2x frequency region are used to determine the true inline strain time series. Fig. 45 presents the twist angles extracted for each sensor location along the riser.

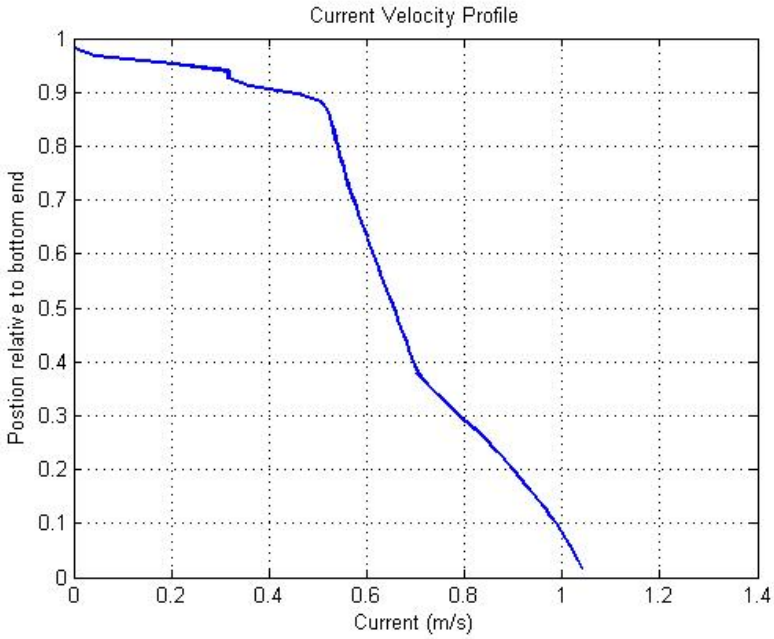

Figure 44. Non-uniform current profile used in Miami2 VIV analysis

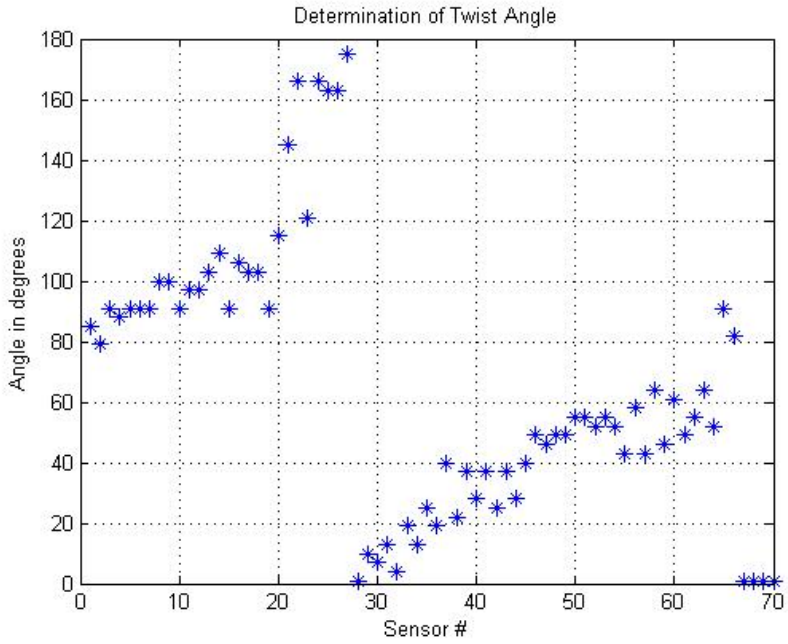

Figure 45. Twist angles calculated from analysis of Miami2 experiments

Numerical Simulation Results

To accurately resolve the inline and crossflow motion of the riser, a finer axial grid resolution was needed. The flow field around the riser was discretized with a structured grid of 180 X 101 X 51 grid elements and the riser grid was discretized using 180 X 182 X 41 grid points. It was realized earlier in the study that the low axial grid resolution with less than 150 segments will not be able to predict the complex dynamics of this extremely long and flexible riser. Therefore, 180 axial segments in flow field and 500 axial segments in the riser geometry were used. Due to this increase in axial segmentation and computational limitations, a coarse resolution of the cross-sectional

grid in inline and transverse direction was adopted. A cross-sectional view of the CFD grid used in this Chapter is presented in Fig. 46.

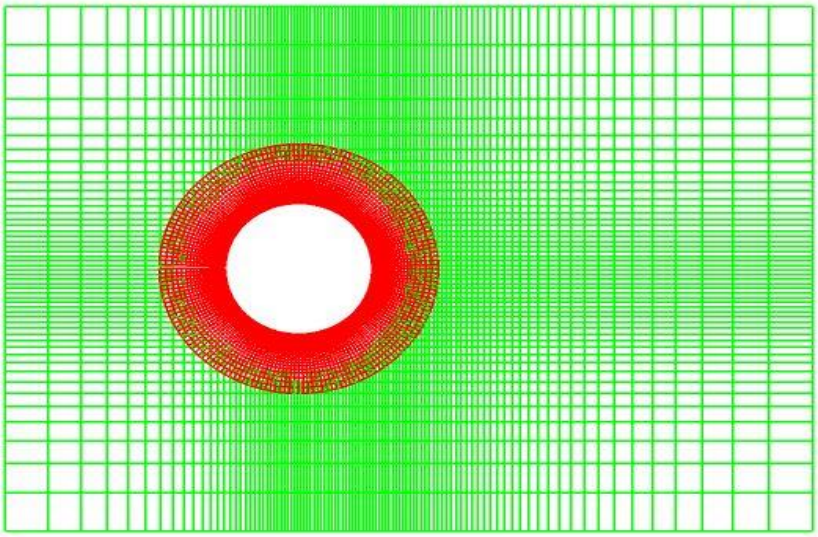

Figure 46. Grid system used in DeepStar Miami2 CFD simulations

A non-uniform velocity as shown in Fig. 44 was applied at the inlet of the grid. The dimensional time step used in this simulation was 0.0007 seconds with a Reynold's number of $3.37 \text{ X } 10^4$. The riser was placed vertically and a linear tension gradient ($dT/dZ \neq 0$) was applied by varying the tension between the weight of the railroad wheel at the bottom and weight of the riser added to railroad wheel weight at the top. It is essential to locate the start and end of each grid system as the current is non-linearly applied and is maximum at the bottom with least tension. The root mean square (RMS) comparison of the strain time series achieved in CFD simulations and extracted from

experimental data is shown in Fig. 47. The plot shows a very good agreement between the FANS CFD results and the experimental data. The CFD simulation over predicts the strain values at the end of the riser which might be a result of the simply supported boundary condition at the end of the riser. The modes acting on the system have zero slopes at the end of the riser and their amplitudes may add up in the vicinity of the boundary resulting in higher riser displacements. Fig. 48 shows the snapshots of VIV evolution at t = 48.8 seconds. The vortices shed aft of the riser follow a '2S' pattern.

A power spectral density analysis of the crossflow strain time series is performed and presented in Fig. 49 and Fig. 50. The peak fundamental frequency observed is ~4.9 Hz and 4.78 Hz from the CFD simulation and the DeepStar Miami2 experiments respectively. Note that Fig. 51 shows only 1x components as the 3x components have been filtered out for the subsequent fatigue calculations.

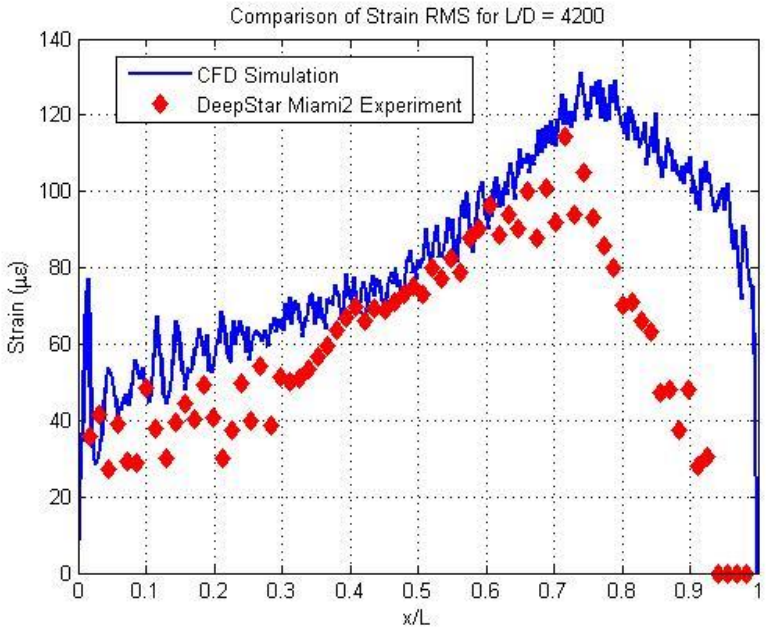

Figure 47. Strain RMS comparison between the CFD simulation and Miami2 expts

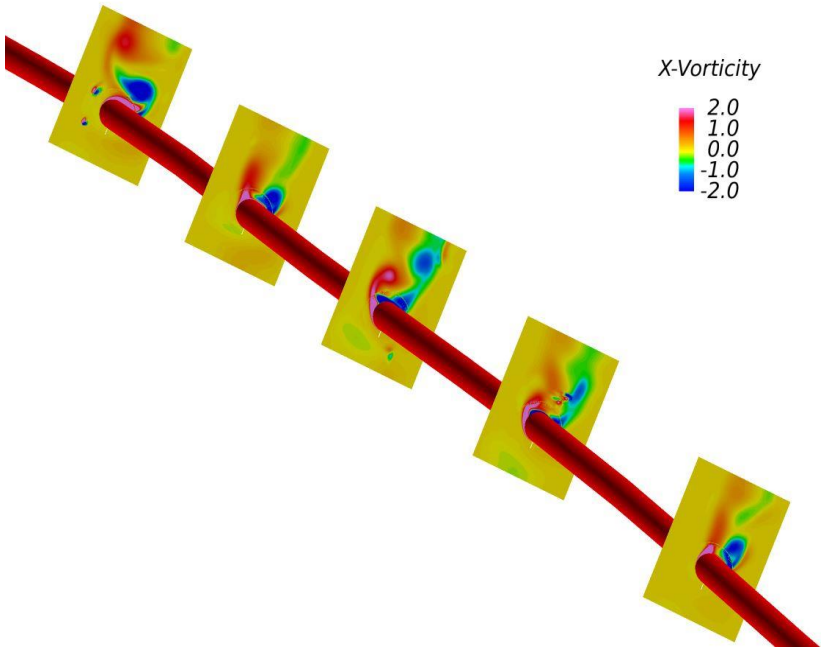

Figure 48. Snapshot of VIV evolution at t = 48.8 secs for non-uniform current

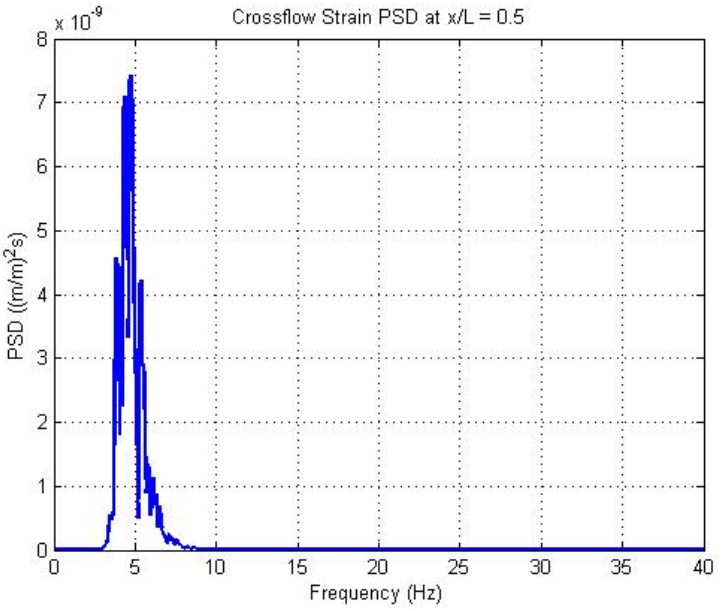

Figure 49. Crossflow strain PSD analysis from CFD simulation

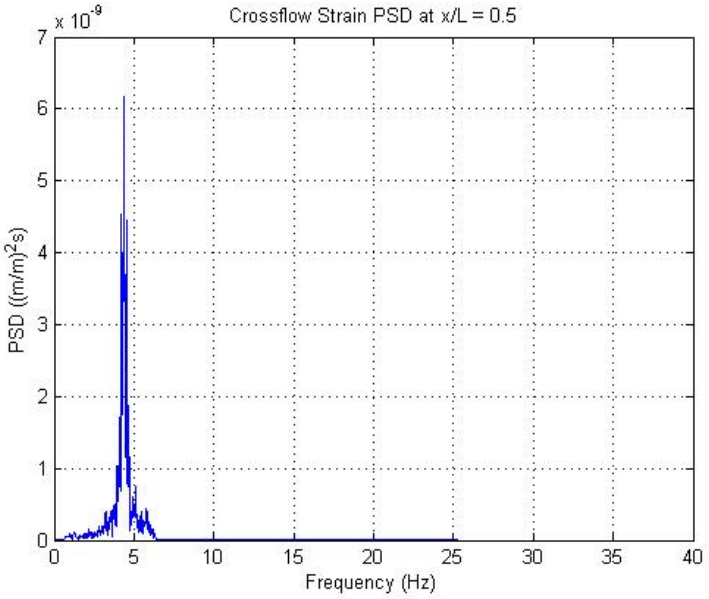

Figure 50. Crossflow strain PSD analysis from DeepStar Miami2 experiments (3x components filtered out)

A modal decomposition method explained in Chapter III of this study has been applied to extract the modal dynamics of the system. The crossflow riser dynamics in CFD simulation is dominated by 10^{th} mode as seen in Fig. 51 and whereas for DeepStar experiments, 8^{th} Mode is dominant shown in Fig. 52. The significant tension variations in the experiments could have affected the modes acting on the system as long risers are tension dominated. Fig. 53 presents the prediction of crossflow fatigue damage from both experimental analysis and CFD simulations. API X' SN curve (Jhingran et al., 2007) has been used in fatigue analysis with a Young's modulus of 200 GPa. The results presented are in a very good comparison.

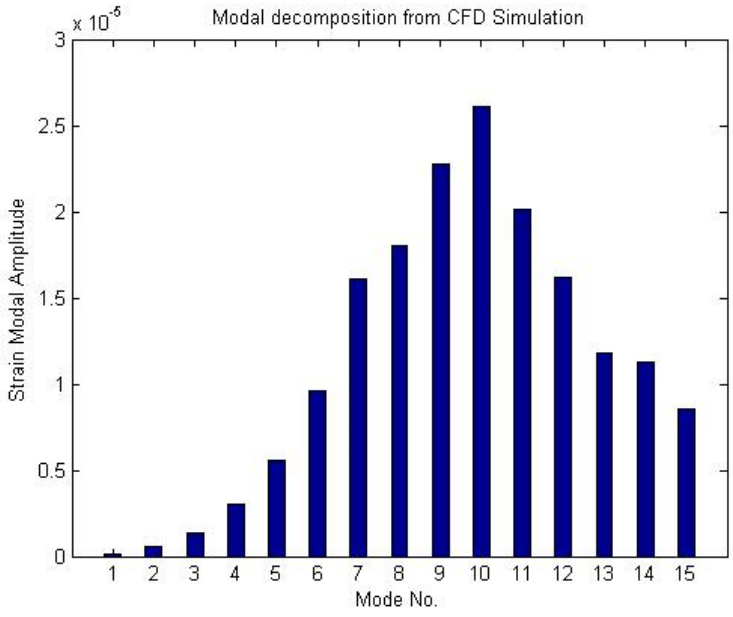

Figure 51. Crossflow strain modal decomposition from CFD simulation

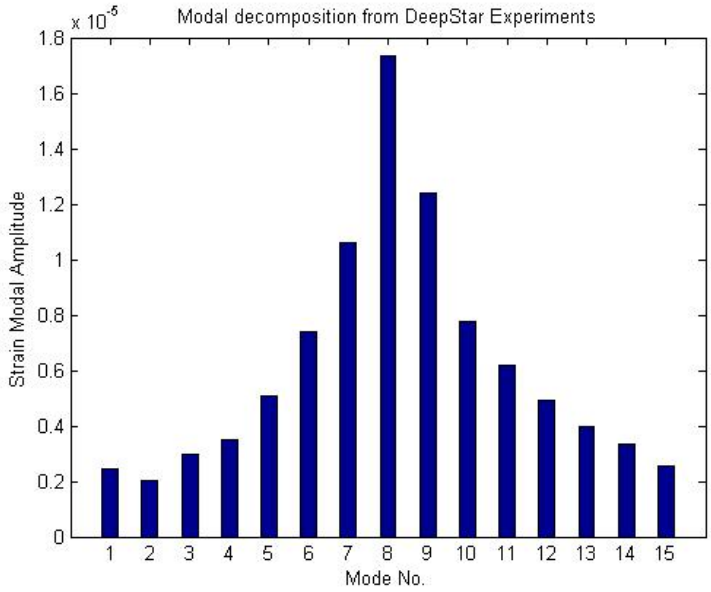

Figure 52. Crossflow strain modal decomposition from DeepStar Miami2 experiments

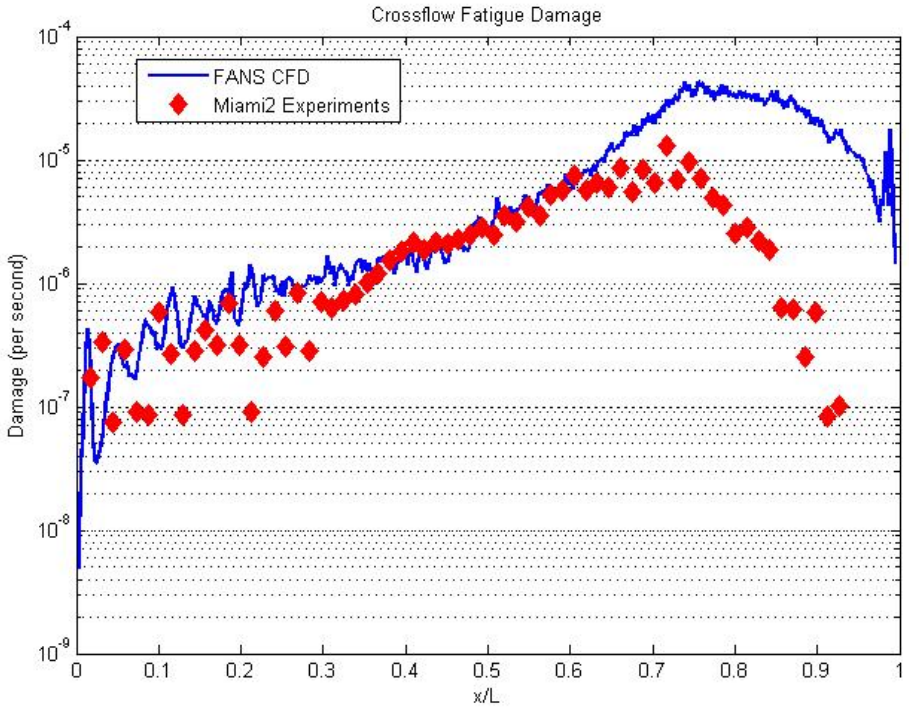

Figure 53. Crossflow fatigue damage comparison of Miami2 data and CFD simulation

CHAPTER VI

CONCLUSION AND DISCUSSION

A fully three dimensional Vortex Induced Vibration Analysis is conducted to study the associated fatigue damage of very long marine risers. The flow field around the riser has been accurately simulated using Finite Analytic Navier-Stokes equations and Large Eddy Simulation Method. The continuity equation is solved using finite volume scheme and the pressure field is updated using a hybrid PISO/SIMPLER algorithm. A tensioned beam motion solver is employed to successfully predict the motion time histories in both inline and crossflow direction for each specified location along the riser. The strain time series is obtained by using a modal extraction method where the modal weights from displacements are used to find the curvature at each point which is subsequently converted to strain. These strain signals are utilized to calculate fatigue damage using a rainflow counting algorithm and Palmgren-Miner's rule. An overset (chimera) grid technique is applied to decompose the flow field and riser in blocks of overlapping grids.

For riser with $L/D \approx 1400$ in uniform flow, four current velocities with $V = 0.3$ m/s, $V = 0.7$ m/s, $V = 1.4$ m/s and $V = 1.7$ m/s were studied and compared to experimental and published data. Two cases with $V = 1.4$ m/s and $V = 1.7$ m/s were studied in detail and the RMS values, PSD functions and fatigue damage along the riser were plotted against experimental data. The results show a very good agreement for both current velocities. All the four current profiles were processed to extract maximum

fatigue damage and were compared with the results published in Trim et al (2005). The lower velocities show a higher fatigue damage prediction from the simulations due to the tendency of the FANS CFD solver to concentrate maximum energy at the 1X component as the higher harmonics are not accurately resolved. The higher velocities (1.4 m/s and 1.7m/s) show under-prediction of maximum fatigue damage due to the problems related to fatigue convergence. Nevertheless, the comparisons are very encouraging.

The riser from NDP experiment with L/D = 1400 is also subjected to a sheared current with a maximum velocity of 0.7 m/s. Both inline and crossflow VIV analysis is presented and compared to test 2350 from NDP 2003 experiments. The RMS motion comparisons show very good agreement between the simulations and experiments for both crossflow and inline motion. The dominant modes and peak frequencies predicted by the FANS CFD are smaller compared to their experimental counterparts which is due to the influence low drift mode acting on the system. The fatigue damage predicted in crossflow direction by CFD compares reasonably well with the experimental data. The inline fatigue damage shows a significant deviation between the two cases which can be attributed to the very brief steady state region achieved in inline direction and the filtering techniques used in the analysis.

The riser geometry from Deepstar Miami2 experiments with L/D ≈ 4200 is also studied in a highly sheared current with maximum velocity of 1.04 m/s. A non-uniform inlet current profile was utilized in FANS CFD solver. Crossflow strain RMS comparisons, Strain PSD functions and fatigue damage comparisons are presented. The results show a reasonable agreement between the experimental data and the numerical

results. However, a finer axial resolution and increase in number of iterations to get a significant steady state region is needed for better resolution of the numerical results.

In conclusion, FANS CFD solver, the riser beam motion solver and fatigue calculation module have been verified for an accurate assessment of VIV fatigue damage in very long marine risers. The modules are also proved to be efficient in handling extremely complex fluid flows with large Reynold's numbers. Using the above study, FANS CFD with the fatigue module can also be successfully applied to other slender marine structures to identify critical fatigue locations and thereby providing a detailed fatigue strength assessment.

REFERENCES

Baarholm, GS, Larsen, CM, and Lie, H (2006). "On fatigue damage accumulation from in-line and cross-flow vortex-induced vibrations on risers," *Journal of Fluids and Structures*, *22*(1), 109–127.

Bearman, PW (1984). "Vortex shedding from oscillating bluff bodies," *Journal of Fluid Mechanics*, *16*, 195–222

Blevins, RD (1990). "Flow-Induced Vibrations," 2nd Edition. Van Nostrand Reinhold, ISBN 0-442-20651-B.

Bourguet, R, Karniadakis, GE, and Triantafyllou, MS (2011). "Lock-in of the vortex-induced vibrations of a long tensioned beam in shear flow," *Journal of Fluids and Structures*, *41*, 33–42.

Constantinides, Y, Oakley, OH (2008). "Numerical Prediction of VIV and Comparison with Field Experiments," Proceedings of the ASME 27th International Conference on Offshore Mechanics and Arctic Engineering (OMAE), Estoril, Portugal.

Govardhan, R, Williamson, CHK (2000). "Modes of Vortex Formation and Frequency Response of a Freely Vibrating Cylinder," Journal of Fluids Mechanics, Vol 420, pp 85-130.

Holmes, S, Oakley, OH, and Constantinides, Y (2006). "Simulation of Riser VIV Using Fully Three Dimensional CFD Simulations," *Volume 4: Terry Jones Pipeline Technology; Ocean Space Utilization; CFD and VIV Symposium*, *2006*, 563–570.

Huang, K, Chen, HC, and Chen, CR (2007). "Riser VIV Analysis by a CFD Approach," *Proceedings of the 17th International Offshore and Polar Engineering Conference*, 2722–2729.

Huang, K, Chen, HC, and Chen, CR (2008). "Riser VIV Induced Fatigue Assessment by a CFD Approach," *Proceedings of the 18th International Offshore and Polar Engineering Conference*, 408-415.

Huang, K, Chen, HC, and Chen, CR (2010). "Vertical riser VIV simulation in uniform current," *Journal of Offshore Mechanics and Arctic Engineering*, 132 (3), 031101.

Huang, K, Chen, HC, and Chen, CR (2011). "Numerical scheme for riser motion calculation during 3-D VIV simulation," *Journal of Fluids and Structures*, 27(7), 947–961.

Huang, K, Chen, HC, and Chen, CR (2012). "Vertical riser VIV simulation in sheared current," *International Journal of Offshore and Polar Engineering*, 22, 142–149

Jhingran, V, and Vandiver, JK (2007). "Incorporating the Higher Harmonics in VIV Fatigue Predictions," *Proceedings of the 26th International Conference on Offshore Mechanics and Arctic Engineering, OMAE2007*(29352), 891–899.

Lie, H, & Kaasen, KE (2006). "Modal analysis of measurements from a large-scale VIV model test of a riser in linearly sheared flow," *Journal of Fluids and Structures*, *22*(4), 557–575.

Lucor, D, Mukundan, H, & Triantafyllou, MS (2006). "Riser modal identification in CFD and full-scale experiments," *Journal of Fluids and Structures*, *22*(6-7), 905–917.

Meneghini, JR, Saltara, F, Fregonesi, RA, Yamamoto, CT, Casaprima, E, Ferrari, JA (2004). "Numerical Simulations of VIV on Long Flexible Cylinders Immersed in Complex Flow Fields," *European Journal of Mechanics B/Fluids,*Vol 23, pp 51-63.

Mukundan, H, Modarres-Sadeghi, Y, Dahl, JM, Hover, FS, and Triantafyllou, MS (2009). "Monitoring VIV fatigue damage on marine risers," *Journal of Fluids and Structures*, *25*(4), 617–628.

Newman, D, and Karniadakis, GE (1996). "Simulations of Flow Over a Flexible Cable: a Comparison of Forced and Flow-Induced Vibration," *Journal of Fluids and Structures*, *10*(5), 439–453.

Newman, DJ, Karniadakis, GE (1997). "Simulations of flow past a freely vibrating cable," *Journal of Fluid Mechanics,* 344, 95–136

Pantazopoulos (1994). "Vortex-induced vibration parameters: Critical review," *Offshore Technology Comference.*

Pontaza, JP, Chen, CR, and Chen, HC (2004). "Chimera Reynolds averaged Navier-Stokes simulations of vortex-induced vibration of circular cylinders," *Proceedings of the International ASCE Conference: Civil Engineering in the Oceans VI*, 166-176.

Pontaza, JP, Chen, CR, and Chen, HC (2005a). "Simulations of high Reynolds number flow past arrays of circular cylinders undergoing vortex-induced vibrations," *Proceedings of the 15th International Offshore and Polar Engineering Conference,* 201-207.

Pontaza, JP, Chen, HC, and Chen, CR (2005b). “Numerical simulations of riser vortex-induced vibrations,” *Proceedings of the 2005 Society of Marine Engineers and Naval Architects (SNAME) Conference*, 52, 1-12.

Pontaza, JP, Chen, HC, and Reddy, JN (2005). “A local-analytic-based discretization procedure for the numerical solution of incompressible flows,” *International Journal for Numerical Methods in Fluids*, 49, 657-699.

Pontaza, JP, and Chen, HC (2007). "Three-Dimensional Numerical Simulations of Circular Cylinders Undergoing Two Degree-of-Freedom Vortex-Induced Vibrations." *Journal of Offshore Mechanics and Arctic Engineering*, 129(3), 158-164.

Suhs, N.E. and Tramel, RW (1991), “PEGSUS 4.0 Users Manual,” Arnold Eng Dev Center Report AEDC-TR-91-8, Arnold Air Force Station, TN.

Thorsen, MJ, Saevik, S, and Larsen, CM (2015). "Fatigue damage from time domain simulation of combined in-line and cross-flow vortex-induced vibrations," *Marine Structures*, *41*, 200–222.

Tognarelli, MA, Taggart, S, Campbell, M (2008). “Actual VIV Fatigue Response of Full Scale Drilling Risers: With and Without Suppression Devices,” *Proceedings of the ASME 27th International Conference on Offshore Mechanics and Arctic Engineering* (OMAE), Estoril, Portugal.

Triantafyllou, M, Triantafyllou, G, Tein, D and Ambrose, BD (1999). "Pragmatic Riser VIV Analysis," *Offshore Technology Connference*, OTC 10931

Trim, AD, Braaten, H, Lie, H, and Tognarelli, MA (2005). "Experimental investigation of vortex-induced vibration of long marine risers," *Journal of Fluids and Structures*, *21*, 335–361.

Vandiver, JK, Jaiswal, V, Swithenbank, SB, and Jhingran, V (2006). "Fatigue damage from high mode number vortex-induced vibration," *Proceedings of the 25th International Conference on Offshore Mechanics and Arctic Engineering*, *OMAE2006*.

Vandiver, JK, Li, L (2003). “Shear7 V4.3 Program Theoretical Manual,” September 2003

Vandiver, JK, Marcollo, H, and Chaurasia, H (2007). "Phenomena observed in VIV bare riser field tests," *Proceedings of the 26th International Conference on Offshore Mechanics and Arctic Engineering*, *OMAE2007*(29562), 1–7.